remote sensing

MDPI

Article

Nearshore Benthic Mapping in the Great Lakes: A Multi-Agency Data Integration Approach in Southwest Lake Michigan

Molly K. Reif [1,*], Brandon S. Krumwiede [2], Steven E. Brown [3], Ethan J. Theuerkauf [4] and Joseph H. Harwood [5]

1 Joint Airborne Lidar Bathymetry Technical Center of Expertise, Environmental Laboratory, U.S. Army Engineer Research and Development Center, 7225 Stennis Airport Road, Suite 100, Kiln, MS 39556, USA
2 Office for Coastal Management, National Ocean Service, National Oceanic and Atmospheric Administration, 31 College Street, Duluth, MN 55812, USA; Brandon.Krumwiede@noaa.gov
3 Illinois State Geological Survey, Prairie Research Institute, University of Illinois at Urbana-Champaign, Champaign, IL 61820, USA; Steebrow@illinois.edu
4 Department of Geography, Environment and Spatial Sciences, Michigan State University, 673 Auditorium Road, East Lansing, MI 48824, USA; Theuerk5@msu.edu
5 Joint Airborne Lidar Bathymetry Technical Center of Expertise, Mobile District, U.S. Army Corps of Engineers, 7225 Stennis Airport Road, Suite 100, Kiln, MS 39556, USA; Joseph.H.Harwood@usace.army.mil
* Correspondence: Molly.K.Reif@usace.army.mil

Abstract: The Laurentian Great Lakes comprise the largest assemblage of inland waterbodies in North America, with vast geographic, environmentally complex nearshore benthic substrate and associated habitat. The Great Lakes Water Quality Agreement, originally signed in 1972, aims to help restore and protect the basin, and ecosystem monitoring is a primary objective to support adaptive management, environmental policy, and decision making. Yet, monitoring ecosystem trends remains challenging, potentially hindering progress in lake management and restoration. Consistent, high-resolution maps of nearshore substrate and associated habitat are fundamental to support management needs, and the nexus of high-quality remotely sensed data with improvements to analytical methods are increasing opportunities for large-scale nearshore benthic mapping at project-relevant spatial resolutions. This study attempts to advance the integration of high-fidelity data (airborne imagery and lidar, satellite imagery, in situ observations, etc.) and machine learning to identify and classify nearshore benthic substrate and associated habitat using a case study in southwest Lake Michigan along Illinois Beach State Park, Illinois, USA. Data inputs and analytical methods were evaluated to better understand their implications with respect to the Coastal and Marine Ecological Classification Standard (CMECS) classification hierarchy, resulting in an approach that could be easily applied to other shallow coastal environments. Classification of substrate and biotic components were iteratively classified in two Tiers in which classes with increasing specificity were identified using different combinations of airborne and satellite data inputs. Classification accuracy assessments revealed that for the Tier 1 substrate component (3 classes), average overall accuracy was 90.10 $\pm$ 0.60% for 24 airborne data combinations and 89.77 $\pm$ 1.02% for 12 satellite data combinations, whereas the Tier 1 biotic component (2 classes) average overall accuracy was 93.58 $\pm$ 0.91% for 24 airborne data combinations and 92.67 $\pm$ 0.71% for 11 satellite data combinations. The Tier 2 result for the substrate component (2 classes) was 93.28% for 2 airborne data combinations and 95.25% for the biotic component (2 classes). The study builds on foundational efforts to move towards a more integrated data approach, whereby data strengths and limitations for mapping nearshore benthic substrate and associated habitat, expressed through classification accuracy, were evaluated within the context of the CMECS classification hierarchy, and has direct applicability to critical monitoring needs in the Great Lakes.

Keywords: benthic mapping; machine learning; Coastal and Marine Ecological Classification Standard (CMECS); airborne hyperspectral imagery; Sentinel-2 imagery; Illinois Beach State Park; southwest Lake Michigan; Coastal Zone Mapping and Imaging Lidar (CZMIL) System

Citation: Reif, M.K.; Krumwiede, B.S.; Brown, S.E.; Theuerkauf, E.J.; Harwood, J.H. Nearshore Benthic Mapping in the Great Lakes: A Multi-Agency Data Integration Approach in Southwest Lake Michigan. *Remote Sens.* **2021**, *13*, 3026. https://doi.org/10.3390/rs13153026

Academic Editors: Tom W. Bell, Kyle C. Cavanaugh, Erin L. Hestir and Joseph D. Ortiz

Received: 30 June 2021
Accepted: 28 July 2021
Published: 1 August 2021

1. Introduction

Lake and ocean bottom, or benthic habitats, are critical zones of interface between the physical processes that shape lake morphology and surface geology and a large number of species that need specific bottom types for shelter, feeding, and reproduction [1]. The Laurentian Great Lakes comprise the largest assemblage of inland waterbodies in North America and are strongly influenced by biological processes associated with the lake floor, which contribute to whole-lake productivity and biodiversity [2]. Many native fishes and other aquatic species have strong associations with substrates for spawning and cover. Simultaneously, the lake bottom is increasingly dominated by benthic invasive species which have induced dramatic whole-lake phase shifts in food webs, water quality, and the fisheries economy [3]. Furthermore, impacts from anthropogenic forces (development, deforestation, shoreline armoring, wetland dewatering, etc.) have resulted in whole-lake changes, such as to chemical, physical, and biological integrity. As a result, the Great Lakes Water Quality Agreement was signed in 1972, amended in 1983 and 1987, and updated again in 2012 to help restore and protect the basin, in which ecosystem monitoring is a key objective for adaptive management, environmental policy, and decision making [4]. However, monitoring ecosystem trends over time remains a challenging task, especially over such a vast geographic, environmentally complex, and dynamic system like the Great Lakes. Specifically, progress in lake and marine coastal ecosystem restoration, monitoring, and management continues to be hindered by a lack of consistent, high-resolution mapping of nearshore substrate and associated habitat, including submerged aquatic vegetation (SAV).

Historically, nearshore substrate and associated habitats have been mapped in a spatially and temporally piece-meal fashion with varying spatial resolution, coverage, and accuracy around the Great Lakes [5]. Data sources typically include discrete bottom grab samples, in situ measurements, and single- and multi-beam depth soundings, while more recent methods, such as satellite and airborne imagery and light detection and ranging (lidar) data, offer repeatable and consistent temporal and spatial coverage. Given environmental variability in the basin and limitations associated with each data collection method, no single solution works well in all areas. Thus, detailed substrate and habitat maps only exist in scattered, isolated areas where data resolution is sufficient, often supporting individual restoration project engineering and design, and the only basin-wide information describing geomorphology, substrate, and habitat is available at a broad scale [6]. Ultimately, this means that data gaps exist, leaving managers without the sufficient spatial, temporal, or data coverage detail needed to describe substrate and habitat features [5]. In order to work towards a solution to overcome these gaps, it will take a multi-data fusion approach, capitalizing on the strengths of individual data collection methods and technologies.

Despite challenges with mapping nearshore benthic substrate and habitat, advancements have been made in the development and application of remote sensing technology for mapping complex coastal and inland waterbodies [7,8]. The first of these advancements is increased spatial coverage of passive electro-optical multi- and hyperspectral imagery with increased spatial, spectral, and temporal resolutions in both airborne and spaceborne platforms. Additionally, there is increased coverage from active sensors, such as airborne lidar and spaceborne radar, in which sensors emit and measure returned light or microwave energy, respectively. For example, integrated airborne sensor suites such as the U.S. Army Corps of Engineers' (USACE) Coastal Zone Mapping and Imaging Lidar (CZMIL) System, operated under the National Coastal Mapping Program (NCMP) by the Joint Airborne Lidar Bathymetry Technical Center of Expertise (JALBTCX), routinely collects high-resolution imagery (<1 m) and topobathymetric lidar for coastal areas of the U.S., including the Great Lakes [9]. Additionally, moderate- and high-resolution satellite multispectral sensors, such as the European Space Agency's Sentinel-2, offers increased spatial coverage at relatively high spatial (10–20 m) and spectral resolutions that help to overcome cloud cover limitations and increased data availability over coastal areas with the

added benefit of broad, public access [10]. Other examples of higher-resolution commercial satellite multispectral sensors that can be used for coastal mapping applications include Maxar WorldView-2 and -3 (~1.2–1.8 m), Airbus Pleiades, and Planet SuperDove satellite constellations [11]. Together, these data help to address the spatial data coverage and resolution gaps; yet, challenges with water column optical properties can confound their use in detailed substrate and habitat mapping [7,12].

The second major advancement in the use of remote sensing for benthic mapping is the enhancement of system hardware and software, leading to improved analytical methods for extracting sea- or lake-bed characteristics. The primary limitations for discriminating different benthic types from imagery is due to the following: spectral heterogeneity of the bottom, depth and water column properties and associated absorption and scattering of light, and the radiometric capabilities of the sensor [7,12,13]. For those reasons, the ability to distinguish benthic types varies across aquatic systems, depths, and water conditions. Kutser et al. [7] provides an extensive review of the evolution of remote sensing technology to map shallow water systems (benthic habitat and bathymetry <20 m in depth). They explain that to help overcome the effect of the water column and obtain information about benthic characteristics, there are empirical, semi-analytical, and analytical processing techniques that can be employed [12]. In general, empirical methods can be site-specific and require appropriately-timed, in situ measurements in the form of ground truth, while more recent analytical, or physics-based inversion, modeling techniques may be less in situ data-dependent but are more computationally complex and reliant upon atmospheric correction of the imagery [7,14]. Inversion-optimization and non-linear optimization techniques established by Brando et al. [15] and Lee et al. [16] continue to be refined and improved [17,18] to help separate benthic target signals from the interference with and optical properties of the water column, especially in complex coastal and inland waterbodies.

Even more numerous than the approaches to overcome water column complexities are the methods with which to identify benthic substrate and habitats from input data (imagery, lidar depth, in situ samples, etc.). The classification of input data can either be unsupervised (no training or ground truth samples) or supervised (manually or semi-automated input of training or ground truth samples). Such methods are often used in remote sensing and can also be directly integrated with empirical, semi-analytical, and analytical approaches for bathymetry and benthic characterization. In general, there are a wide variety of supervised classification techniques used to characterize benthic features, such as traditional pixel-based classifiers like Maximum Likelihood [19,20], machine learning algorithms like Support Vector Machine or Random Forest [21,22], Object-Based Image Analysis (OBIA), a knowledge-based classification approach [23,24], and ensemble classification approaches [23,25,26]. Often classification techniques make use of multiple data inputs, fusing various passive (electro-optical imagery) and active (lidar) to help increase map accuracy and detection capabilities [8,27]. All of these techniques have had varying degrees of success and accuracy for mapping benthic substrate and habitat with most applications related to mapping the distribution of coral reef, SAV, and macroalgae [7,12]. In the Great Lakes specifically, the use of passive and active remote sensing data for nearshore benthic mapping applications have focused on such topics as monitoring the movement of legacy mine tailings and impacts to local fisheries [28], habitat monitoring around National Lakeshores [29,30], marine sanctuary planning [31], and SAV mapping, such as nuisance algae *Cladophora* [32].

While no one data type and analytical approach works well in all areas of the Great Lakes, the convergence of increasing amounts of remotely sensed data with improvements to methods is opening opportunities to develop more frequent large-scale nearshore benthic mapping at project-relevant spatial resolutions. To that end, the current trend is moving towards integrating various available data, maximizing their individual strengths based on location and environmental condition, as well as establishing semi-automated or automated analytical methods that can be consistently applied for more comparable and repeatable

map results [22]. While the studies referenced thus far have shown success in that direction, the goal of basin-wide nearshore benthic mapping is still considered premature, with data and technical approaches requiring refinement and vetting by the user community (researchers, coastal managers, etc.). In particular, the need to understand the character of the nearshore benthic environment in the Great Lakes rises from management topics related to recreation, sport fishing, shoreline erosion, beach maintenance, infrastructure improvements, ecosystem restoration, and beneficial re-use of dredged material. Decisions made without adequate inventory or characterization of coastal habitats (terrestrial and benthic), information about erodibility of the lake-bed substrate, or knowledge of the interplay between the shoreline and the nearshore benthic environment under different lake levels and weather scenarios, can negatively impact coastal habitat, shoreline change rates, lake-bed down cutting, and longshore sediment transport regimes. Decision making is further confounded by a multitude of private, local, state, and federal jurisdictions. Methods that enhance or facilitate lake-bed classification, in a consistent manner, and across the Great Lakes are therefore needed to facilitate cross-jurisdiction collaboration and problem solving. As such, the goals of this study are to build on existing approaches to:

1. Evaluate the integration and role of high-fidelity data (airborne imagery and lidar, satellite imagery, in situ observations, etc.) using machine learning (Support Vector Machine) to identify nearshore benthic substrate and associated habitat and to better understand their implications with respect to the Coastal and Marine Ecological Classification Standard (CMECS) classification system hierarchy;
2. Develop a semi-automated, repeatable approach that could be applied in other shallow coastal environments using a case study in southwest Lake Michigan, USA.

2. Materials and Methods

2.1. Study Area

For this study, an 11.7 square kilometer area in southwest Lake Michigan along Illinois Beach State Park, Illinois was selected (Figure 1). It falls within Lake County, just north of the heavily populated Cook County (Chicago's North Shore) and just south of the Wisconsin state line. As noted in Mwakanyamale et al. [33] the southwest Lake Michigan shoreline has experienced periods of erosion due in part to impacts from anthropogenic activity and development together with recent high lake levels. The study area, while currently in a more natural, state-owned park setting, historically experienced urban housing development and construction of a military base during low lake levels (1915–1975), followed by severe shoreline erosion during periods of high lake levels, at which point shoreline armoring and protection structures and infrastructure along the immediate shoreline were destroyed with remnants currently submerged in the nearshore part of the study area [33]. The area was selected for this study in part because it is the site of on-going shoreline mapping to better understand regional sediment transport with coordinated efforts conducted between the Illinois Coastal Management Program, Illinois State Geological Survey (ISGS), USACE, the National Oceanic and Atmospheric Administration (NOAA), and other local partners. As such, it provides an ideal opportunity to maximize a variety of on-going data collection activities. While the majority of the study area consists of unconsolidated sand, it is marked by the unique anthropogenic remnants described earlier, patches of substrate (coarse gravel fields), and biotic (*Cladophora* sp. macroalgae and quagga mussels [Dreissena rostriformis bugensis]) features, and sporadic cultural features (shipwrecks). This is consistent with the nearby Wisconsin—Lake Michigan lake-bed characterization conducted by NOAA in fulfillment of the proposed sanctuary [31].

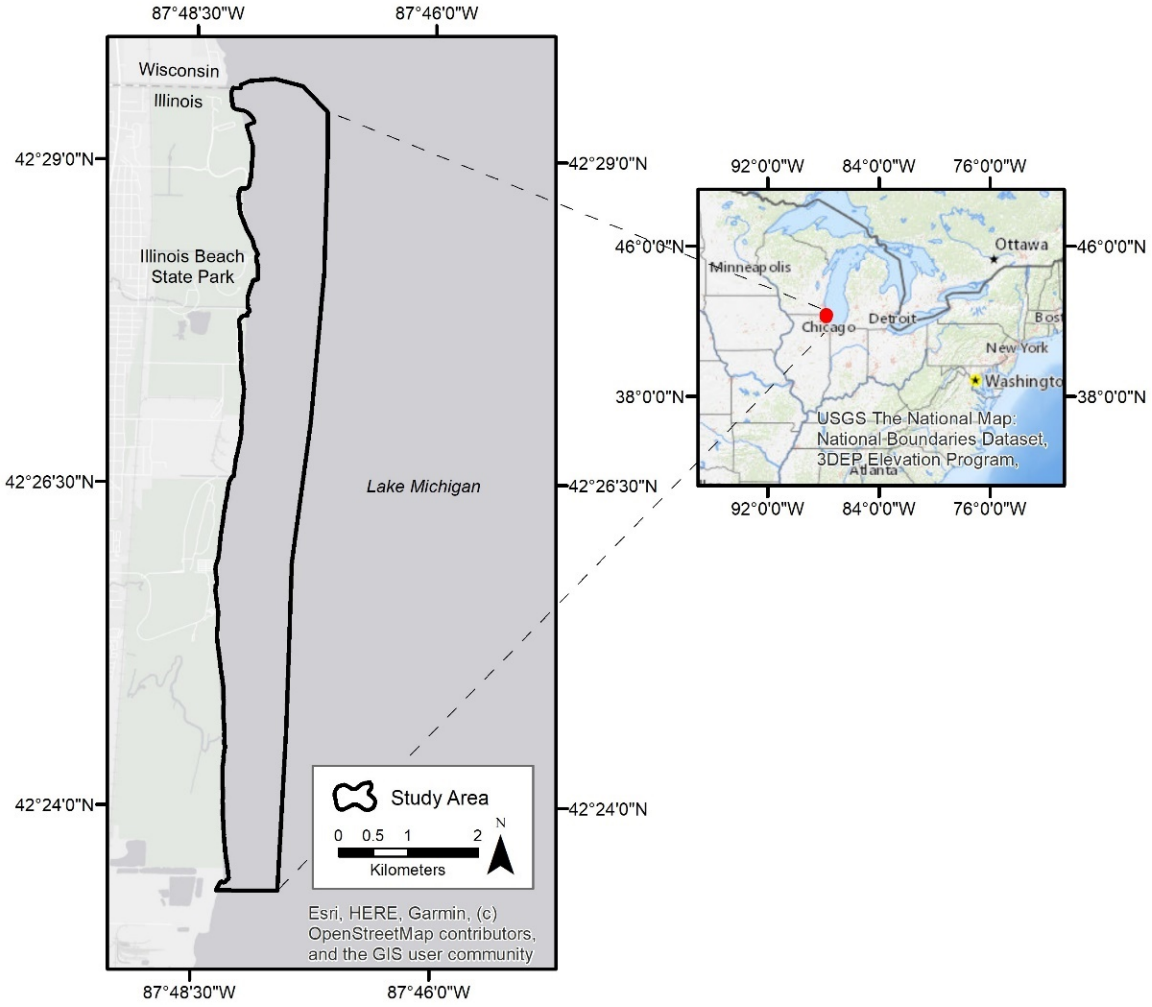

Figure 1. Study area at southwest Lake Michigan, USA.

2.2. Airborne Data Pre-Processing

Airborne hyperspectral imagery (HSI) and topobathymetric lidar data were collected by the JALBTCX over the study area using the CZMIL system. This system is an integrated sensor suite that includes a circular scanning lidar system, an Itres Compact Airborne Spectrographic Imager (CASI)-1500 hyperspectral sensor, and a true-color digital frame Phase One 150 MP camera with a sensor fusion concept for improved coastal mapping (benthic classification, water column characterization, etc.) in challenging shallow water environments that are often turbid or have breaking waves [34,35]. Eight shore-parallel flights were flown at 400 m altitude on 17 July 2018 on a fixed-wing aircraft. The CASI-1500 was programmed to collect 48 spectral bands (375–1050 nanometers; 14 nanometer bandwidth) at 1 m spatial resolution, offering advantages with high spectral resolution (narrow bands) that have shown utility for seafloor mapping in shallow, turbid waters [8,9,12,19,23]. Topobathymetric lidar data were collected using the Teledyne Optech CZMIL Nova system including 10 kHz bathymetric full waveform lidar (green laser in the 532 nanometer wavelength) with the effective rate increased to 70 kHz on land and in optically shallow water using a segmented detector [34]. The CZMIL collected lidar data with topographic and shallow channel bathymetric point densities of 2 points per square meter (nominal point spacing of 0.7 m) and deep channel bathymetric point densities of 0.25 points per square meter (nominal point spacing of 2 m); in this region, the CZMIL switched from shallow to deep channel coverage at approximately the 9 m depth mark. Unlike passive sensors, active sensor technology like lidar measures time of flight from light pulses emitted from

the sensor to estimate depth using the 532 nanometer (green) wavelength for seafloor applications [8,9]. Maximum possible depth for this survey occurred at 14 m (±0.5 m).

Both the HSI and topobathymetric lidar data were pre-processed using Teledyne's HydroFusion software and the standard National Research Council's Committee on Data Management and Computation (CODMAC) levels for HSI and lidar data pre- and post-processing as well as product generation to prepare data for analysis. For the HSI, HydroFusion standard pre-processing procedures included (1) radiometric calibration (conversion of digital numbers to at-sensor radiance), (2) geometric correction for distortion removal using topobathymetric lidar data, (3) water glint and ripple correction, (4) atmospheric correction to surface reflectance adapted from the Simple Model of the Atmospheric Radiative Transfer of Sunshine (SMARTS) model [36] developed by the National Renewable Energy Laboratory [37] resulting in a 1 m spatial resolution mosaicked image (personal communication Joseph H. Harwood, USACE). HydroFusion software was also used to conduct standard lidar pre-processing in which lidar point clouds were classified and used to generate seamless topobathymetric first return and bare earth digital elevation model grids at 1 m spatial resolution. Additional products generated from the standard products in HydroFusion software included the following: (1) bathymetry grid, (2) water-leaving hyperspectral reflectance image (atmospherically corrected reflectance; water surface and water column were not removed) with 29 spectral bands between 375 and 780 nanometers (spectral subset from the 48 bands), and a (3) fusion image (atmospherically corrected with sun glint and water ripples, water surface rugosity, removed and scaled and resampled to match the lidar depth grid) with 48 spectral bands between 380 and 1050 nanometers (Figure 2, panels a–c). The water-leaving reflectance (WLR) and fusion (FU) images were further transformed to reduce data dimensionality and noise using the Minimum Noise Fraction (MNF) transform tool in ENVI v5.5 (L3Harris Geospatial, Boulder, Colorado) software. Specifically, this transformation is often applied to hyperspectral imagery to reduce the number of spectral bands in which two principal components transformations are used to isolate and reduce noise, likewise reducing computational requirements [38]. Using the software-recommended number of spectral bands to retain important spectral information, the reduced images resulted in 23 MNF bands for the WLR image and 10 MNF bands for the FU image. Lastly, a lidar reflectance image was generated from the bathymetry, illustrating relative seafloor reflectance at 532 nanometers, following the model developed in Tuell et al. [39] with improvements specific to CZMIL lidar data (e.g., radiometric calibration and optimized calibration coefficients, implementation of a radiometric balancing channel to account for inhomogeneity in the return intensity across shallow channels, and improved color and flight line balancing, Figure 2, panel d). All images and grids were resampled to 3 m spatial resolution to strike a balance between spatial detail and computational intensity, clipped to the study area, ranging from the high-water line onshore (176 m contour obtained from the elevation grid) to approximately 10 m depth offshore, and consolidated in a layer stack for use in image classification analysis.

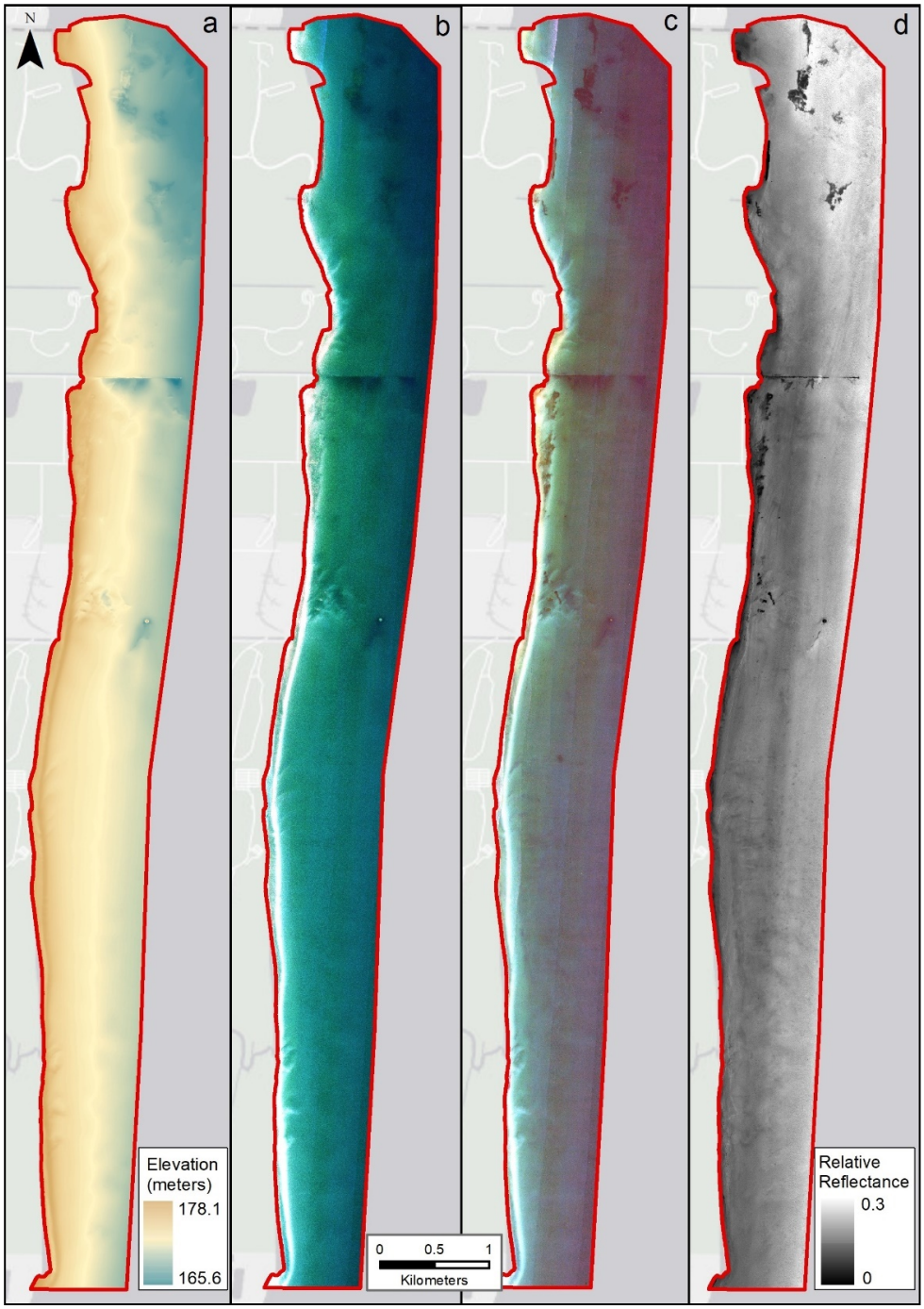

Figure 2. Airborne data products: (**a**) bathymetry, (**b**) hyperspectral water-leaving reflectance, (**c**) fusion, and (**d**) bathymetric reflectance.

2.3. Satellite Data Pre-Processing

The European Space Agency's Sentinel-2B multispectral imagery was acquired over the study area on 10 July 2018 (S2B_MSIL1C_20180710T163839_N0206_R126_T16TDN). This scene was selected as it was the closest in temporal proximity to the airborne lidar and hyperspectral imagery data collection acquisition. The Level 1C processed product, top of atmosphere (TOA) reflectance, was downloaded from the Copernicus Open Access Hub [40] and processed using Version 7.0.0 of Sentinel Application Platform (SNAP) software [41]. Prior to utilizing the imagery within the Sen2Coral toolbox, the imagery was processed to the 2A product level, bottom of atmosphere (BOA) reflectance with terrain and cirrus cloud corrections. While atmospheric correction procedures are an important aspect of pre-processing and have direct bearing on reflectance products, it was not our intent to evaluate their influence on benthic mapping, as previously explored in Wicaksono et al. [22] and Song et al. [42]. In contrast, our aim was to examine the performance of readily available and open data products and software that can be used in basin-wide benthic mapping strategies. As a result, the Sen2Cor280 algorithm was used within the SNAP software to develop BOA reflectance and applied to the imagery. Upon completion, all bands were resampled to 10 m spatial resolution and subset to the study area.

The Sen2Coral toolbox v1.1 [43] within SNAP was used to generate both a Depth Invariant Index (DII) and Empirical Bathymetry, or Satellite-Derived Bathymetry (SDB), grids for use in the classification. The methodology provided in the Copernicus Research and User Support for Sentinel Core Products Sen2Coral training [43] was applied to help with deglinting and masking of land, clouds, and surface waves present in the BOA reflectance imagery. The DII was derived by using the Lyzenga [44] and Green et al. [45] methods in which reflectance attenuation is approximately an inverse exponential with water depth. The SDB was derived by using the Stumpf et al. [13] method in which water reflectance attenuation varies between different wavelengths captured in the satellite bands and determining the ratio between the bands with depth to develop relative bathymetry. Bathymetric points were selected from the airborne lidar point cloud that fell within the study area in which 935 points were used to train and develop the SDB product. Afterwards, an additional 2000 randomly sampled points were used to validate the resulting SDB against the airborne bathymetric lidar point cloud. All satellite products developed for classification input are shown in Figure 3, panels a–c.

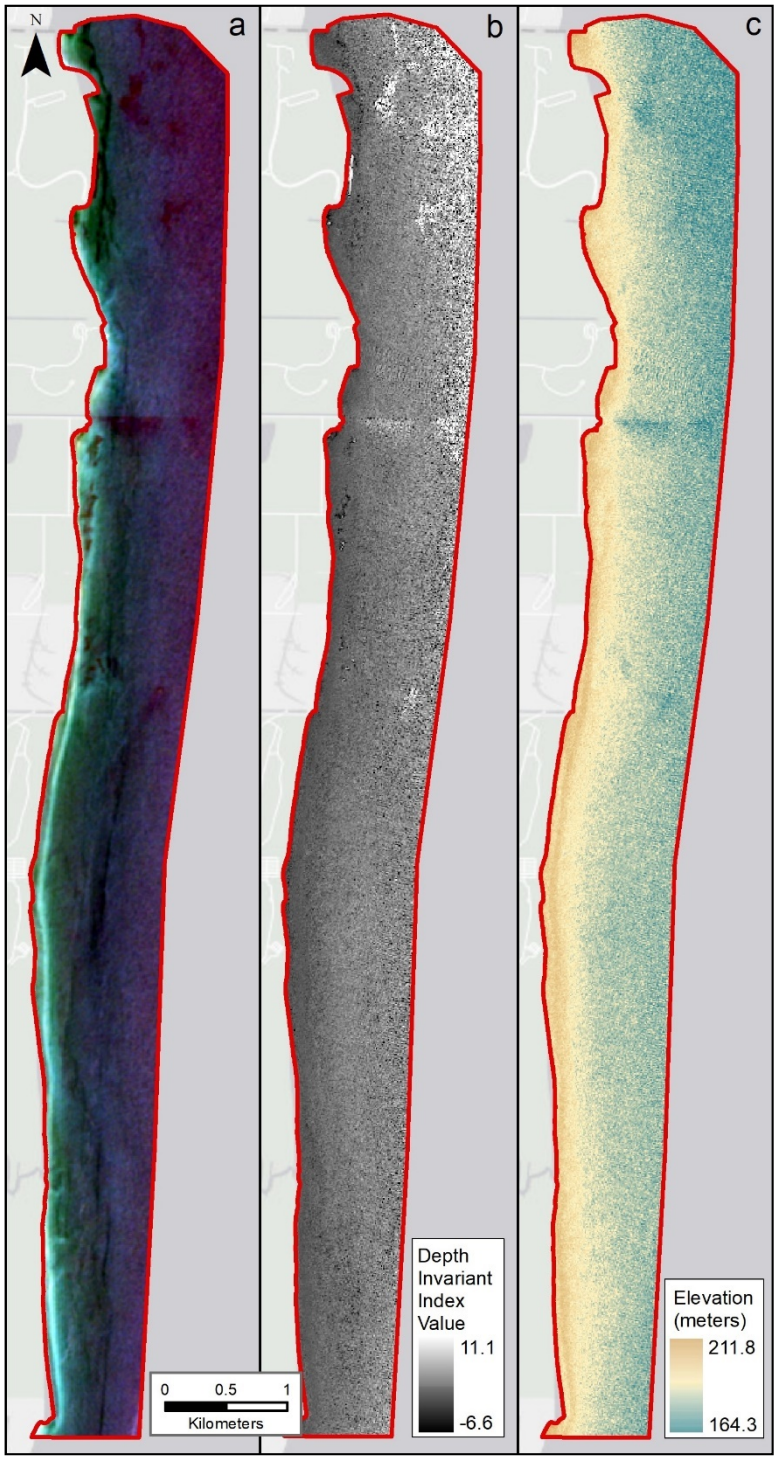

Figure 3. Satellite data products: (**a**) multispectral (bottom of atmosphere) reflectance, (**b**) Depth Invariant Index, and (**c**) Satellite-Derived Bathymetry.

2.4. Field Data Collection

As part of on-going shoreline mapping in the region, ISGS collected initial ground truth data at 24 random points within the study area from 11 to 12 July 2018 including sediment grab samples (with grain size classifications), drop camera photographs (Garmin Virb XE 1080pHD camera), sidescan sonar (Lowrance HDS7 Carbon sonar), and single-beam bathymetry (Seafloor Systems Dual Frequency 30/200 kHz single-beam echosounder). Upon review of the initial ground truth data, subsequent ground truth data were collected by ISGS in targeted areas to expand coverage of anticipated bottom types during the

summer and fall of 2019. This included multi-beam bathymetry for qualitative assessment using a kit with the following specifications:

Applanix-Trimble POS MV V4 kit:
GPS antennae (2): Trimble GPS Zephyr model 2
topside processor: PCS-29 Wavemaster
Inertial Motion Unit: POS MV V4
Reson-Teledyne SeaBat 7125 kit:
Receiver: RESON EM7200–1 7125.7128 200/400 kHz
Projector: RESON TC2181 7125 200 and 400 kHz
RESON SVP 71; 2000 m; EM 7223 sound velocity probe
RESON SeaBat 7125 MBES Processor Unit
SVP-15 sound velocity kit:
SVP-15 Sound velocity probe
RESON SVPD-10 Power and Control Unit
Universal Sonar Mount, standard mount with gear drive
Acquisition software:
QPS Quincy: integration of MBES, GPS, and sound velocity data
Trimble Applsanix GNSS Surfer: for real-time GPS correction
Trimble VRSNow: real-time RTK broadband GPS correction services
Boat: Kann 8.2 m flat bottom work skiff

Subsequent ground truth data collection also included lake-bottom videography along transects using an AquaVu 1080i Pro camera kit. Lake-bottom videography was collected using an AquaVu 1080i Pro camera kit. The camera cable was tethered to a steel davit cable weighted by a 12-pound river anchor with a carabineer to eliminate offset in the camera location, similar to a down-rigger setup used in salmon fishing on the Great Lakes. The anchor tether reduced offset (blowback or angle) of the camera relative to the boat position. The anchor depth was controlled, and the camera depth was independently controlled below the anchor depth by manually lifting and lowering the camera cable based on a real-time visual view of camera output. Live video output from the AquaVu topside monitor was fed to a computer using a HDMI video cable connected to a Magewell USB Capture 4K Plus device. Topside environmental conditions (e.g., boat motion) and boat crew narration were captured with a Microsoft HD Cinema Cam connected to the computer and mounted in an aft ceiling position inside the boat cabin. Boat position, heading, and water depth were derived from the boat navigation system which included a Garmin 6212 chartplotter, Garmin GPS 19× HVS GPS antenna, Garmin GSD 22 Remote Sounder, and Garmin basic dual frequency (50/200 kHz) transducer. GPS and sounder data were exported from the chartplotter in NMEA 0183 format with a serial cable connected from the chartplotter to the computer. Franson GPS Gate software enabled a virtual COM port on the computer for real-time GPS, heading, speed, and time display in ArcGIS 10.5.1 for Desktop with the GPS toolbar. Open Broadcast Studio (OBS) software installed on the computer collected the AquaVu and web cam video feeds, an ArcGIS data layout window showed live boat navigation tracks and bathymetry. The OBS software setting saved video frames at a rate of 30 frames per second. In addition, the NMEA 0183 data strings from the chartplotter were independently saved with HyperTerminal software in ASCII text format. The NMEA data strings were post-processed to identify video start, video roll, and video stop records based on the GPS time stamp identified in the video display and the matching time stamp in the NMEA 0183 data log. Because the ArcGIS GPS dialogue window showed GPS location and time, each video frame, or group of a few frames, were cross-referenced to the boat navigation track. Thus, a coordinate for each video frame was provided. Because boat heading is recorded, the camera view shed was known at all times. Video transects consisted of regularly spaced track log locations (points) minimally 0.5 m apart and resulted in approximately 4500 GPS locations of bottom image videos used to characterize bottom features. Ground truth points from both field campaigns

were randomly selected and divided approximately in half for image classification and validation analysis tasks (Figure 4).

Figure 4. Field data collected in July 2018 and summer and fall 2019 used for image classification and validation.

2.5. Data Classification and Analysis

2.5.1. Classification System

For this study, the Coastal and Marine Ecological Classification Standard (CMECS) was used to classify field and remotely sensed data. This system offers an approach for classifying estuarine, coastal, and open-ocean environments, including options for classifying one or more components: water column, geoform, substrate, and biotic [46]. It is also established as a federal standard compliant with the Federal Geographic Data

Committee's (FGDC) national standards, and due to its flexible structure, it is well suited for cross-walking to other classification systems, such as those reviewed in Strong et al. [47]. For this study, the substrate and biotic components were selected to illustrate nearshore benthic features and because these two components have hierarchical structures, the level of classification specificity can be directly linked to the amount of data detail in which it is based upon. Additionally, the system allows for the combination of components, such as co-existing features and modifiers, to increase the level of classification specificity and accuracy. Figure 5 illustrates the hierarchical structure for both components as well as an example for each corresponding unit. Due to challenges related to limited occurrences of certain bottom types or field samples of certain bottom types, thus limited training samples within the study area, a tiered approach was applied to the CMECS structure to assist with better understanding the performance of various remote sensing data inputs. Table 1 lists the hierarchical CMECS components, units, descriptions, classification Tier, corresponding class value (identified by class tier index number), and whether classes had corresponding field observations used in this study. The tiered approach allowed for an iterative examination of remotely sensed data inputs as it related to classification accuracy. As a result, tiered CMECS classes with corresponding short names and class values (class tier index numbers) were mapped as follows in Figure 6 with sample underwater photos for each class depicted in Figures 7 and 8.

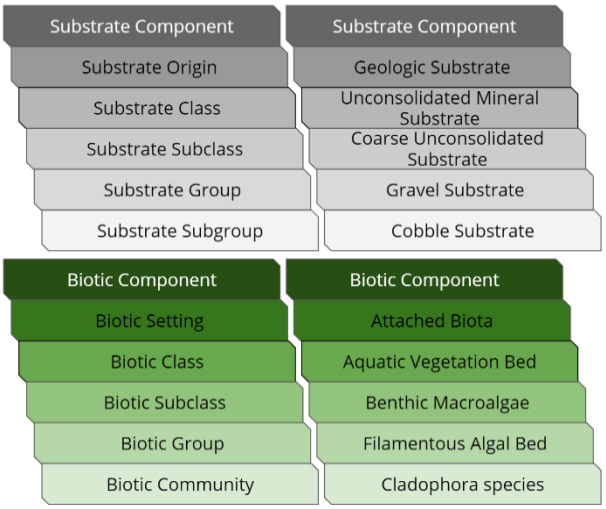

Figure 5. Hierarchical structure of the substrate and biotic components within the Coastal and Marine Ecological Classification Standard (CMECS), including individual units (**left**) and class examples (**right**).

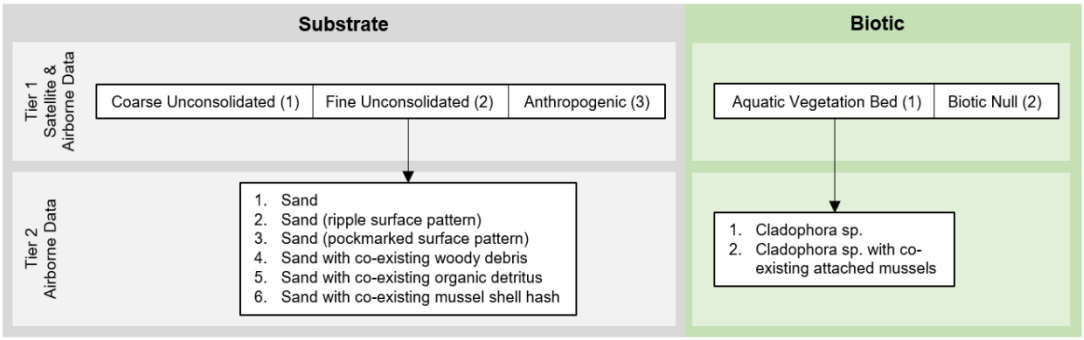

Figure 6. Tiered CMECS class short names and class values (class tier index numbers).

Table 1. CMECS components, units, descriptions, classification tier, corresponding class value (identified by class tier index number), and classes with corresponding field observations used in this study. Class tier index numbers correspond to short class names in Tables 2 and 3 (# = number).

CMECS Hierarchy	CMECS Code	CMECS Description	Class Tier 1 Index #	Class Tier 2 Index #	Field Observation
Substrate Component					
Substrate Origin	S1	Geologic Substrate	—	—	—
Substrate Class	S1.2	Geologic Substrate | Unconsolidated Mineral Substrate	1	X	Yes
Substrate Subclass	S1.2.1	Geologic Substrate | Unconsolidated Mineral Substrate | Coarse Unconsolidated Substrate	—	—	—
Substrate Group	S1.2.1.1	Geologic Substrate | Unconsolidated Mineral Substrate | Coarse Unconsolidated Substrate | Gravel Substrate	1	X	Yes
Substrate Group	S1.2.1.1/S2.5.3.3	Geologic Substrate | Unconsolidated Mineral Substrate | Coarse Unconsolidated Substrate | Gravel Substrate (COE: Mussell Shell Hash)	1	X	Yes
Substrate Subgroup	S1.2.1.1.1	Geologic Substrate | Unconsolidated Mineral Substrate | Coarse Unconsolidated Substrate | Gravel Substrate | Boulder Substrate	1	X	Yes
Substrate Subgroup	S1.2.1.1.2	Geologic Substrate | Unconsolidated Mineral Substrate | Coarse Unconsolidated Substrate | Gravel Substrate | Cobble Substrate	1	X	Yes
Substrate Subgroup	S1.2.1.1.2/S2.5.3.3	Geologic Substrate | Unconsolidated Mineral Substrate | Coarse Unconsolidated Substrate | Gravel Substrate | Cobble Substratestrate (COE: Mussel Shell Hash)	1	X	Yes
Substrate Group	S1.2.1.2	Geologic Substrate | Unconsolidated Mineral Substrate | Coarse Unconsolidated Substrate | Gravel Mixes Substrate	1	X	Yes
Substrate Subgroup	S1.2.1.3.2	Geologic Substrate | Unconsolidated Mineral Substrate | Coarse Unconsolidated Substrate | Gravelly | Gravelly Muddy Sand	1	X	Yes
Substrate Subgroup	S1.2.1.3.2/S2.5.3.3	Geologic Substrate | Unconsolidated Mineral Substrate | Coarse Unconsolidated Substrate | Gravelly Substrate | Gravelly Muddy Sand (COE: Mussel Shell Hash)	1	X	Yes
Substrate Subclass	S1.2.2	Geologic Substrate | Unconsolidated Mineral Substrate | Fine Unconsolidated Substrate	—	—	—
Substrate Group	S1.2.2.1	Geologic Substrate | Unconsolidated Mineral Substrate | Fine Unconsolidated Substrate | Slightly Gravelly Substrate	—	—	—
Substrate Subgroup	S1.2.2.1.1	Geologic Substrate | Unconsolidated Mineral Substrate | Fine Unconsolidated Substrate | Slightly Gravelly Substrate | Slightly Gravelly Sand	2	1	Yes
Substrate Subgroup	S1.2.2.1.1(SP04)	Geologic Substrate | Unconsolidated Mineral Substrate | Fine Unconsolidated Substrate | Slightly Gravelly Substrate | Slightly Gravelly Sand (Surf Pattern: Ripple Surface)	2	2	Yes
Substrate Subgroup	S1.2.2.1.1(SP07)[P]	Geologic Substrate | Unconsolidated Mineral Substrate | Fine Unconsolidated Substrate | Slightly Gravelly Substrate | Slightly Gravelly Sand (Surf Pattern: Pockmarked Surface Pattern)	2	3	Yes

Table 1. *Cont.*

CMECS Hierarchy	CMECS Code	CMECS Description	Class Tier 1 Index #	Class Tier 2 Index #	Field Observation
Substrate Subgroup	S1.2.2.1.1/S2.3.1.2	Geologic Substrate | Unconsolidated Mineral Substrate | Fine Unconsolidated Substrate | Slightly Gravelly Substrate | Slightly Gravelly Sand (COE: Woody Debris)	2	4	Yes
Substrate Subgroup	S1.2.2.1.1/S2.3.2	Geologic Substrate | Unconsolidated Mineral Substrate | Fine Unconsolidated Substrate | Slightly Gravelly Substrate | Slightly Gravelly Sand (COE: Organic Detritus; Possible INT: Spotted Surface Color)	2	5	Yes
Substrate Subgroup	S1.2.2.1.1/S2.5.3.3	Geologic Substrate | Unconsolidated Mineral Substrate | Fine Unconsolidated Substrate | Slightly Gravelly Substrate | Slightly Gravelly Sand (COE: Mussel Shell Hash)	2	6	Yes
Substrate Origin	S3	Anthropogenic Substrate	—	—	—
Substrate Class	S3.1	Anthropogenic Substrate | Anthropogenic Rock Substrate	—	—	—
Substrate Subclass	S3.1.2	Anthropogenic Substrate | Anthropogenic Rock Substrate | Anthropogenic Rock Rubble Substrate	3	X	Yes
Substrate Subclass	S3.1.2/S2.3.1.2	Anthropogenic Substrate | Anthropogenic Rock Substrate | Anthropogenic Rock Rubble Substrate (COE: Woody Debris)	3	X	Yes
Substrate Subclass	S3.2.1	Anthropogenic Substrate | Anthropogenic Wood Substrate | Anthropogenic Wood Reef Substrate (INT: Shipwreck SC-419)	3	X	Yes
Substrate Subclass	S3.2.1/S3.4.2	Anthropogenic Substrate | Anthropogenic Wood Substrate | Anthropogenic Wood Reef Substrate (COE: Sparse Metal Substrate; INT: Shipwreck Solon H. Johnson)	3	X	Yes
Substrate Subclass	S3.4.1	Anthropogenic Substrate | Anthropogenic Metal Substrate | Anthropogenic Metal Reef Substrate	3	X	Yes
Substrate Subclass	S3.4.1/S3.2.2	Anthropogenic Substrate | Anthropogenic Metal Substrate | Anthropogenic Metal Reef Substrate (COE: Wood Rubble Substrate)	3	X	Yes
Biotic Component					
Biotic Setting	B2	Benthic/Attached Biota	—	—	—
Biotic Class	B2.5	Benthic/Attached Biota | Aquatic Veg Bed	—	—	—
Biotic Subclass	B2.5.1	Benthic/Attached Biota | Aquatic Veg Bed | Benthic Macroalgae	—	—	—
Biotic Group	B2.5.1.4	Benthic/Attached Biota | Aquatic Veg Bed | Benthic Macroalgae | Filamentous Algal Bed	—	—	—
Biotic Community	B2.5.1.4.4	Benthic/Attached Biota | Aquatic Veg Bed | Benthic Macroalgae | Filamentous Algal Bed | *Cladophora* sp	1	1	Yes
Biotic Community	B2.5.1.4.4/B2.2.2.21.3[P]	Benthic/Attached Biota | Aquatic Veg Bed | Benthic Macroalgae | Filamentous Algal Bed | *Cladophora* sp. (COE: Attached Mussels; PCT cover 9–11)	1	2	Yes
	Biotic Null	No Biota Observed	2	X	Yes

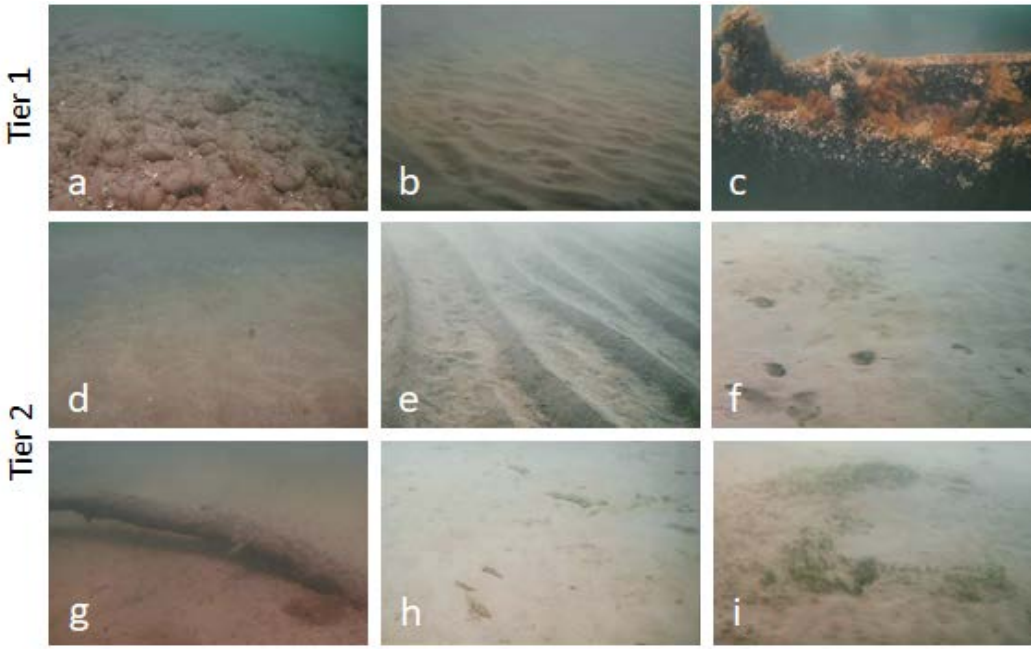

Figure 7. Underwater photo samples for Tier 1 substrate classes: (**a**) coarse unconsolidated, (**b**) fine unconsolidated, and (**c**) anthropogenic; Tier 2 fine unconsolidated substrate classes: (**d**) sand, (**e**) sand (ripple surface pattern), (**f**) sand (pockmarked surface pattern), (**g**) sand with co-existing woody debris, (**h**) sand with co-existing organic detritus, and (**i**) sand with co-existing mussel shell hash.

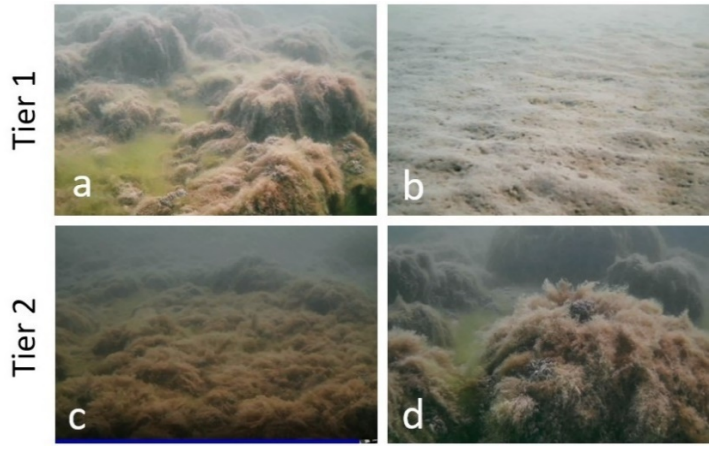

Figure 8. Underwater photo samples for Tier 1 biotic classes: (**a**) aquatic vegetation bed and (**b**) biotic null; Tier 2 aquatic vegetation bed biotic classes: (**c**) *Cladophora* sp. and (**d**) *Cladophora* sp. with co-existing attached mussels.

In Tier 1, three classes were selected for the substrate component and two classes were selected for the biotic component based upon benthic variability represented by the frequency and distribution of ground truth samples within the study area for both the 3 m airborne and 10 m satellite data. More information about the ground truth sample data is provided in the Field Data Classification Section 2.5.2. More specifically, this meant that two Tier 1 substrate classes were characterized at the CMECS subclass level (coarse and fine unconsolidated), while one Tier 1 substrate class was characterized at the CMECS origin level (anthropogenic); two Tier 2 biotic classes were characterized at the CMECS group level (aquatic vegetation bed and biotic null). For the substrate component, only the fine unconsolidated Tier 1 class could be further discriminated into

detailed Tier 2 classes (CMECS substrate subgroup level), in which the resultant classified area had ground truth samples with sufficient class variation (six Tier 2 classes possible). Conversely, the coarse unconsolidated and anthropogenic Tier 1 classes could not be further discriminated into detailed Tier 2 classes because the ground truth samples in those resultant classified areas only represented a single class type and lacked additional class variability for further expansion. For the biotic component, the aquatic vegetation bed Tier 1 class was further discriminated into detailed Tier 2 classes (CMECS biotic community level) in which there were two Tier 2 classes possible with ground truth samples illustrating additional class variability. Additionally, only the 3 m airborne data were used to evaluate Tier 2 classifications since the 10 m satellite did not have sufficient spatial resolution to resolve more detailed bottom types. More information about the classification methods is provided in the Remote Sensing Classification Section 2.5.3.

2.5.2. Field Data Classification

Drop camera photos and sediment grain size classifications from the July 2018 survey and video track log locations from the summer and fall 2019 surveys were used to classify ground truth points with the appropriate Tier 1 and 2 classification codes (Tables 2 and 3). The CMECS Coding System Approach and corresponding Code Set [48] was used to apply the codes to the points. In general, the videos were linked to the point locations using time-stamp information and then bottom points were attributed based on video reviews and interpretation with consensus among researchers. Points were separated approximately in half between samples used in classification versus validation as well as by CMECS component, substrate versus biotic. The points set aside for classification were used to create regions of interest (ROIs) or training samples required for supervised classification techniques. More specifically, ROIs represent the ground truth points in the form of grid cells corresponding to the pixel size of the 3 m airborne or 10 m satellite classification input imagery and data. In some cases, more than one ground truth point fell within a 3 m or 10 m grid cell area, and thus, more than one point described an ROI. In those cases, an ROI cell was attributed with the class code of the majority of points within that cell unless in special cases where the number and type of points were equally split and best judgment was used to define classes in those cases. In total, the 2018 and 2019 points were combined into a comprehensive and classified ground truth ROI dataset for use in image classification and validation.

Table 2. Number of ground truth points (samples) for classification and validation used for Tier 1 classification of the 3 m airborne and 10 m satellite data (# = number).

Short Name (Index #)	# of Classification Samples (3 m)	# of Validation Samples (3 m)	# of Classification Samples (10 m)	# of Validation Samples (10 m)
Substrate Component				
Coarse Unconsolidated (1)	52	46	19	14
Fine Unconsolidated (2)	540	540	182	178
Anthropogenic (3)	38	34	13	10
TOTAL	630	620	214	202
Biotic Component				
Aquatic Vegetation Bed (1)	50	50	19	17
Biotic Null (2)	575	575	190	190
TOTAL	625	625	209	207

Table 3. Number of ground truth points (samples) for classification and validation used for Tier 2 classification of the 3 m airborne data (# = number).

Short Name (Index #)	# of Classification Samples (3 m)	# of Validation Samples (3 m)
Fine Unconsolidated (Substrate Component)		
Slightly Gravelly Sand (1)	501	502
Slightly Gravelly Sand/Surf Pattern: Ripple Surface (2)	3	4
Slightly Gravelly Sand/Surf Pattern: Pockmarked Surface Pattern (3)	17	16
Slightly Gravelly Sand/COE: Woody Debris (4)	1	0
Slightly Gravelly Sand/COE: Organic Detritus; Possible INT: Spotted Surface Color (5)	10	12
Slightly Gravelly Sand/COE: Mussel Shell Hash (6)	2	2
TOTAL	534	536
Aquatic Vegetation Bed (Biotic Component)		
Cladophora sp. (1)	3	5
Cladophora sp./COE: Attached Mussels (2)	15	17
TOTAL	18	22

2.5.3. Remote Sensing Classification

Satellite and airborne data inputs were iteratively classified to examine their impact on classification accuracy for discriminating CMECS-defined classes. Figure 9 shows the overall remote sensing workflow, illustrating the pre-processing, classification inputs, and classification and analysis approach. Image classification was conducted using the data inputs described in the Airborne and Satellite Data Pre-processing Sections (Sections 2.2 and 2.3). Table 4 provides a summary of the satellite and airborne classification inputs. While the goal of this study was not to conduct a full evaluation of analytical methods, initial investigation of Maximum Likelihood (ML) and Support Vector Machine (SVM) classifiers was conducted to determine the best approach for the study area as well as could be easily applied in other coastal environments. Ultimately, ML was not selected for further analysis because initial results showed consistent over- or under-class estimation, resulting in major errors despite attempts to adjust settings, ROIs, etc. This is consistent with similar studies [22], which explain that there are limitations associated with ML when the distribution of the spectral response is not normal (typically the case for benthic environments). Thus, machine learning techniques, such as SVM, which are not based on distribution assumptions, can help overcome those limitations and have shown success in benthic mapping applications [21–23,49]. As with Wicaksono et al. [22], a pixel-based classification approach was selected over OBIA to take advantage of higher spatial resolution data and unique spectral characteristics associated with the airborne and satellite data used as input for identifying detailed benthic features.

Table 4. Summary of satellite and airborne classification inputs.

Classification Inputs	Collection Date	Spatial Resolution (m)
Satellite (S2)		
S2 Multispectral (MS) [Bands 2–5, 8]	10 July 2018	10
Depth Invariant Index (DII)	10 July 2018	10
Satellite-Derived Bathymetry (SDB)	10 July 2018	10
Airborne (AB)		
CASI (CA) Minimum Noise Fraction (MNF) Fusion (FU) [Bands 1–10]	17 July 2018	3
CA MNF Water-Leaving Reflectance (WLR) [Bands 1–23]	17 July 2018	3
AB Lidar Bathymetry [Depth] (DE)	17 July 2018	3
AB Lidar Relative Bathymetric Reflectance (RF)	17 July 2018	3

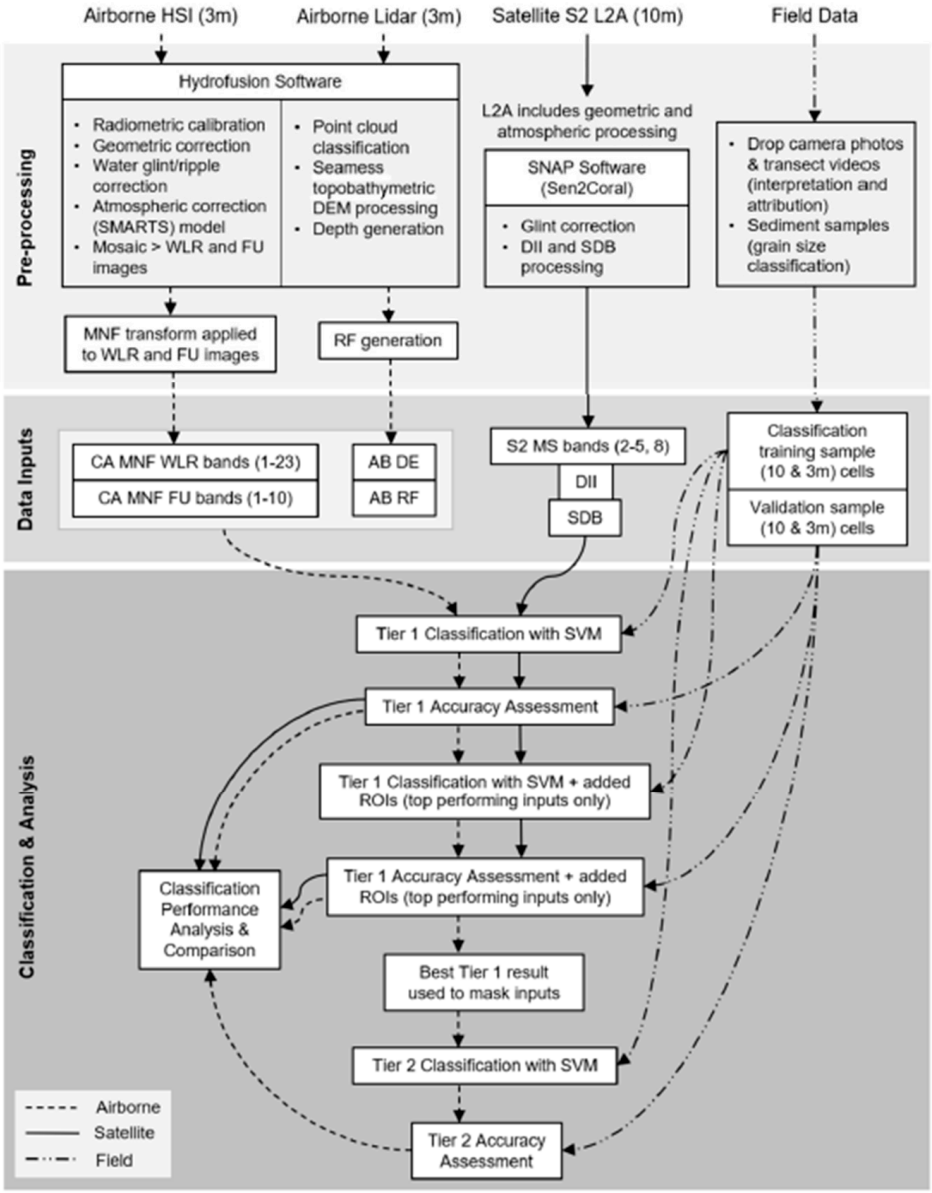

Figure 9. Remote sensing workflow illustrating pre-processing, classification inputs, and classification and analysis approach (HSI = hyperspectral; SMARTS = Simple Model of the Atmospheric Radiative Transfer of Sunshine; DEM = digital elevation model; WLR = water-leaving reflectance; FU = fusion; MNF = Minimum Noise Transform; CA = CASI; DE = lidar depth; RF = bathymetric reflectance; S2 MS = Sentinel-2B Multispectral; DII = Depth Invariant Index; SDB = Satellite-Derived Bathymetry; SVM = Support Vector Machine; and ROIs = regions of interest).

Classification training samples or ROIs (Section 2.5.2. Field Data Classification) were designated in the SVM classifier using ENVI v5.5 software (Kernel Type: Radial Basis Function, Gamma in Kernel Function: 0.029, and Penalty Parameter 100) to identify the Tier 1 biotic and substrate classes (Table 2) applied to different combinations of airborne and satellite data inputs. An accuracy assessment was conducted using an error matrix method comparing resultant classifications with the corresponding 3 and 10 m validation sample datasets (Section 2.5.2. Field Data Classification) to produce overall accuracy, Kappa Coefficient (KC), and producer and user accuracies per class [50]. Upon reviewing initial results, some misclassifications were observed in areas with limited ground truth data, such as areas immediately adjacent to the shoreline (i.e., overclassification of aquatic vegetation bed). Therefore, additional ROIs were manually delineated in misclassified areas using

local knowledge and applied to input data combinations with the highest overall classification accuracies. More specifically, for the Tier 1 classification of the biotic component using airborne data, the following ROIs were added: 10 biotic null (concentrated along the shoreline and some offshore areas) and 11 aquatic vegetation bed (near existing ground truth, but not overlapping with validation data). While multiple attempts at additional ROIs in the classification of the biotic component using satellite data were made, none were successful in resolving misclassifications and were ultimately not used. For the Tier 1 classification of the substrate component using airborne data, the following ROIs were added: 4 coarse unconsolidated (near existing ground truth, but not overlapping with validation data), 21 fine unconsolidated (concentrated along the shoreline and some offshore areas), and 17 anthropogenic (near existing ground truth or known anthropogenic features that lacked ground truth, such as a submerged breakwater). For the Tier 1 classification of the substrate component using satellite data, the following ROIs were added: 14 coarse unconsolidated (near existing ground truth, but not overlapping with validation data) and 7 fine unconsolidated (concentrated along the shore and some offshore areas). No additional ROIs were added to the anthropogenic class in the satellite data classification because the inputs were insufficient for discriminating those features.

The result from the best-performing 3 m airborne Tier 1 classification was used to mask the input data for the Tier 2 classifications of the fine unconsolidated (substrate) and aquatic vegetation bed (biotic) classes. More specifically, the three airborne data combinations with the highest overall accuracy achieved in Tier 1 were evaluated in the SVM classifier for Tier 2 using training samples or ROIs designated in Table 3 (Section 2.5.2. Field Data Classification). No additional ROIs were required in the Tier 2 classification. As with the Tier 1 results, an accuracy assessment was conducted for Tier 2. Satellite data inputs were not able to be further classified in Tier 2 due to spatial resolution limitations associated with the satellite imagery. After accuracy assessments were completed, classification performance (overall and producer accuracies) was evaluated by comparing results to better understand the impact of satellite and airborne data inputs on classification accuracy as related to CMECS class detail.

3. Results

3.1. Classification Performance Analysis

3.1.1. Substrate Component Classification Results

Tier 1 Substrate

For the Tier 1 substrate component, there were a total of 24 airborne data combinations with an average overall accuracy of 90.10 $\pm$ 0.60%, while there were a total of 12 satellite data combinations with an average overall accuracy of 89.77 $\pm$ 1.02% (including data combinations with additional ROIs). In comparison, KCs were more moderate to low, averaging 0.47 ($\pm$0.08) for airborne data combinations and 0.30 ($\pm$0.03) for satellite data combinations. Table A1 (Appendix A) lists the percent overall accuracy and KC, as well as the percent area and producer and user accuracies for the three classes (coarse unconsolidated, fine unconsolidated, and anthropogenic) using airborne and satellite data combinations. The Index field in Table A1 (Appendix A) is a numerical value that is referenced in Figures 10–12 in which classification performance is plotted (percent overall accuracy compared to percent producer accuracy) to help illustrate patterns with respect to unique data combinations. Comparison of classification results is presented for each component by data type in the following sections.

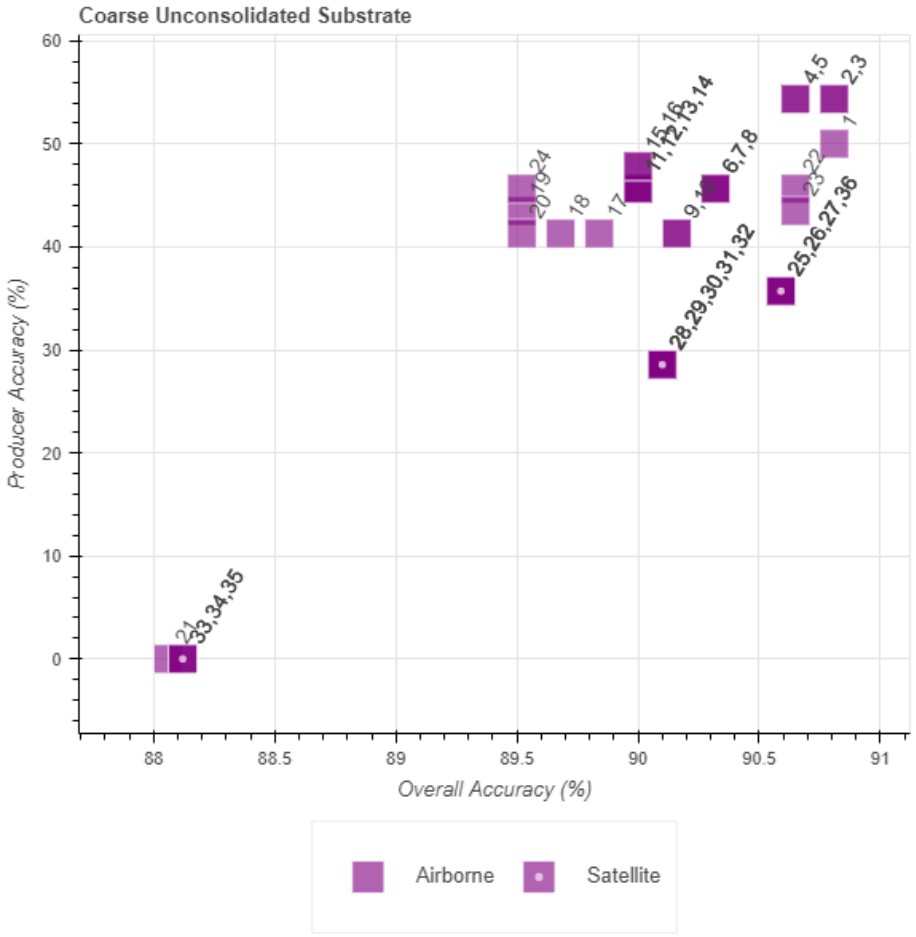

Figure 10. Tier 1 plot of coarse unconsolidated substrate classification performance, comparing percent overall accuracy and percent producer accuracy for airborne and satellite data combinations. Number labels refer to unique classification input data combinations identified in the Index field in Table A1, Appendix A.

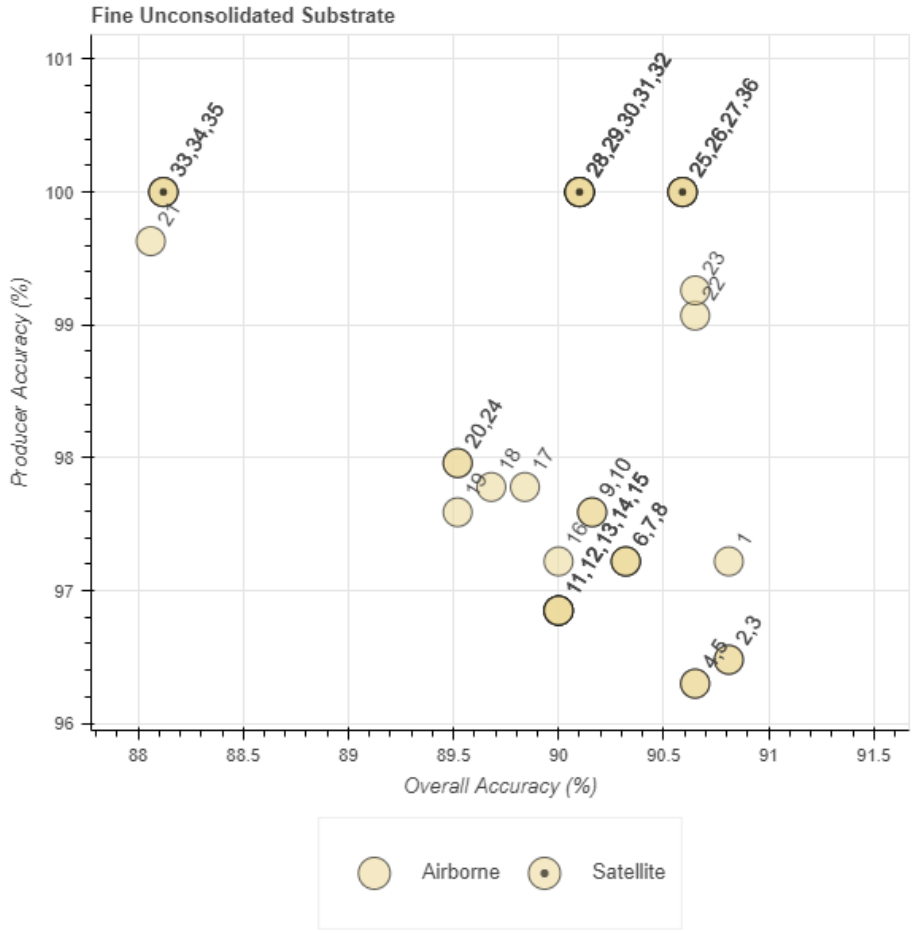

Figure 11. Tier 1 plot of fine unconsolidated substrate classification performance, comparing percent overall accuracy and percent producer accuracy for airborne and satellite data combinations. Number labels refer to unique classification input data combinations identified in the Index field in Table A1, Appendix A.

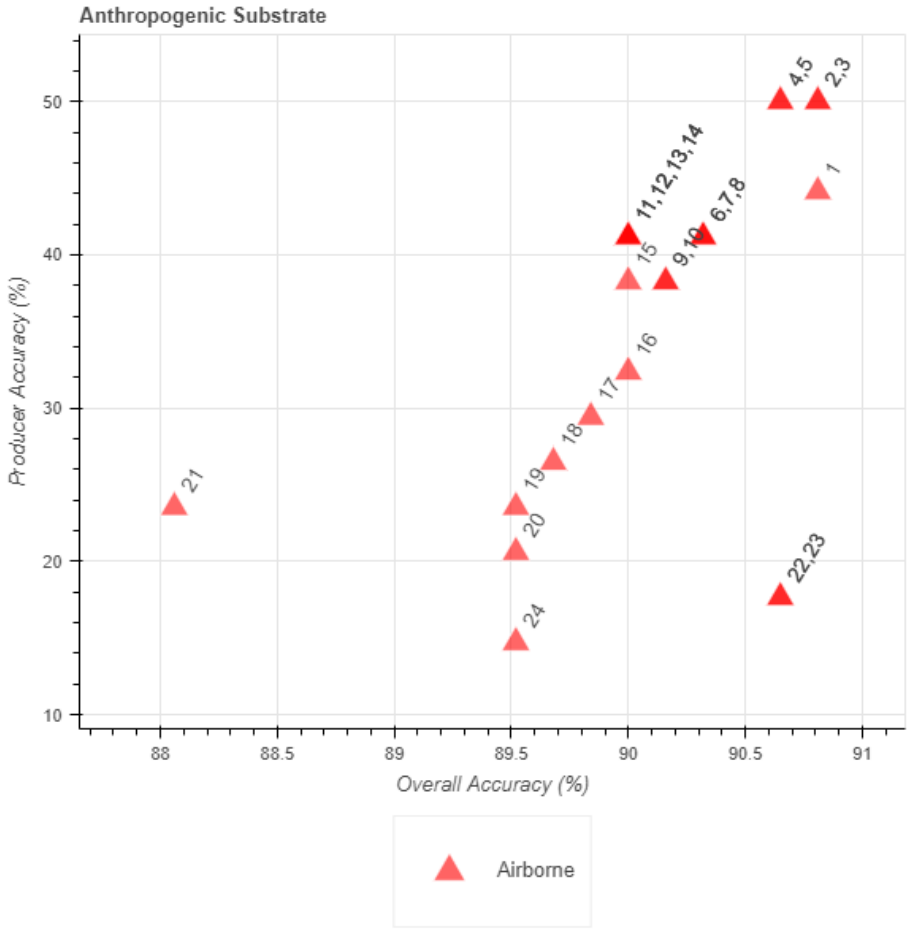

Figure 12. Tier 1 plot of anthropogenic substrate classification performance, comparing percent overall accuracy and percent producer accuracy for airborne only data combinations. Number labels refer to unique classification input data combinations identified in the Index field in Table A1, Appendix A. Note that satellite classification of anthropogenic substrates is not included because the satellite inputs were insufficient for discriminating those features.

In general, the classifications showed that the majority of the area had fine unconsolidated substrate with airborne data combinations estimating 92.51% (±1.91%) and satellite data combinations estimating a higher coverage amount of 98.35% (±1.02%). While the southern part of the study area consisted mostly of fine unconsolidated substrate, pockets of coarse unconsolidated substrate were observed primarily in the northern part of the study area, generally ranging from 0.3 to 0.7 km offshore (airborne data combinations estimated 4.69 ± 0.56% versus satellite data combinations, which estimated approximately half that amount, 2.20 ± 0.26%). Anthropogenic substrate was also found in central and northern parts of the study area, such as a nearshore breakwater, remnant road beds, structures, and debris (ranging from 0.1 to 0.2 km offshore), an intake pipeline (extending 0.9 km in length), a power plant water intake structure (0.75 km offshore), and two shipwrecks (south of the central intake pipeline), with an overall total estimated cover of 3% (±1.04%) from airborne data combinations only. Satellite data were insufficient for classification of anthropogenic substrate (Figure 13; Table A1, Appendix A).

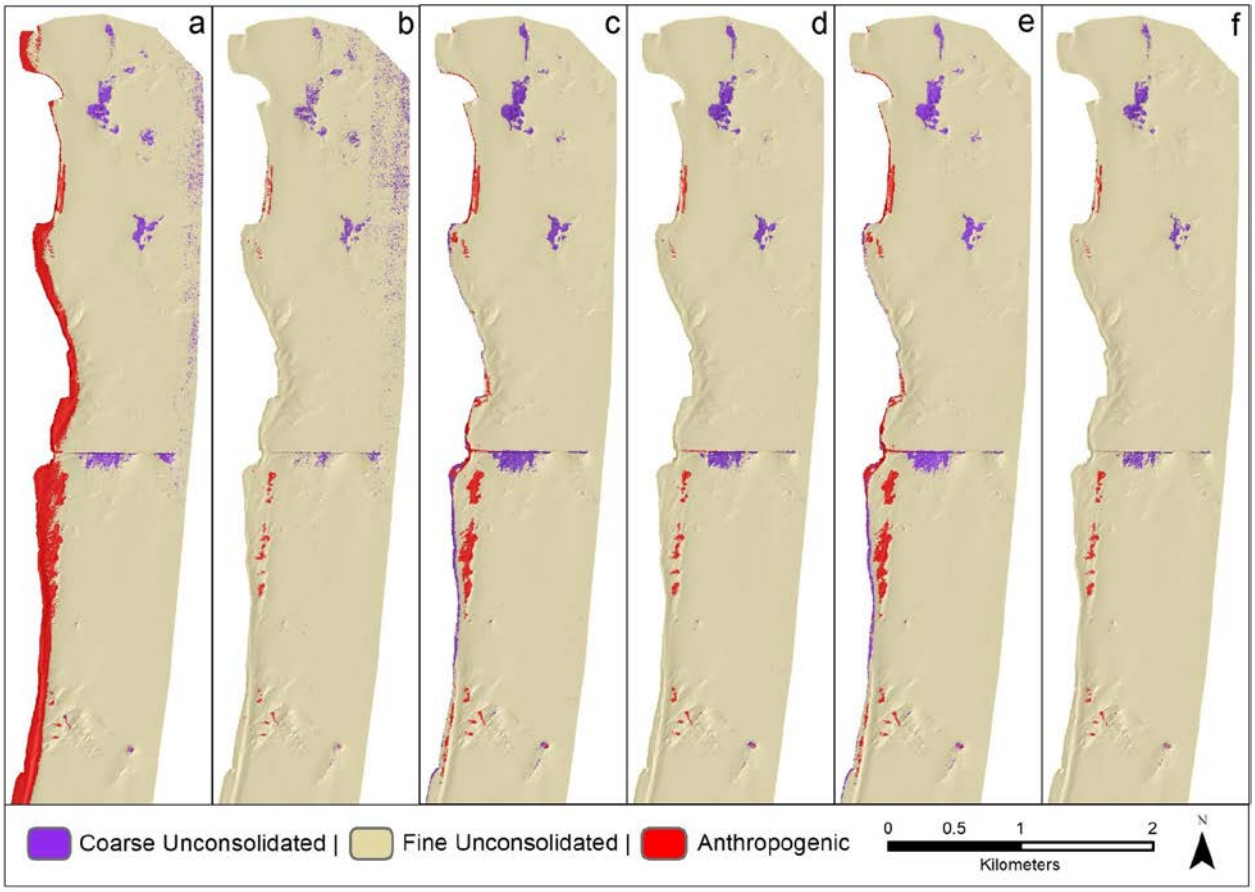

Figure 13. Tier 1 substrate component classification results using airborne data combinations for the north-central section of the study area: (**a**) CA MNF FU, (**b**) CA MNF FU with additional ROIs, (**c**) CA MNF FU + CA MNF WLR, (**d**) CA MNF FU + CA MNF WLR with additional ROIs, (**e**) CA MNF WLR + CA MNF FU + AB DE, and (**f**) CA MNF WLR + CA MNF FU + AB DE with additional ROIs.

The three airborne data combinations with the highest overall classification accuracies included the following (highest to lowest): (1) CA MNF FU, (2) CA MNF FU + CA MNF WLR (and reverse order), and (3) CA MNF WLR + CA MNF FU + AB DE (and reverse order). In general, for most of the top-performing airborne data combinations, data input order did not affect classification accuracy, and thus, combinations with the same data inputs performed the same regardless of order. The top three data combinations with the additional ROIs were also evaluated for accuracy performance, and in cases where data combinations using the same data inputs resulted in redundant classification accuracies (e.g., varying only by data input order), only one of the data combinations was evaluated (i.e., CA MNF FU + CA MNF WLR and CA MNF WLR + CA MNF FU + AB DE). Figure 13 illustrates the classification results of the top three performing data combinations with and without additional ROIs for the north-central section of the study area. The southern section is not shown since it is mostly fine unconsolidated substrate. Two data combinations with additional ROIs (Figure 13, panels b and d) experienced a slight decrease in overall accuracy percent by 0.16% and 1.29%, respectively, while one remained unchanged (Figure 13, panel f), as a result of a lack of validation ground truth data in misclassified areas. However, the amount of area originally misclassified as coarse unconsolidated and anthropogenic in the nearshore (Figure 13, panels a, c and e) decreased, resulting in increased area correctly classified as fine unconsolidated (Table A1, Appendix A). As a result, the producer accuracy for the fine unconsolidated class increased, and although it decreased for the coarse unconsolidated and anthropogenic classes, the user accuracies for those two classes increased (Figures 10–12). Despite the lack

of validation ground truth data in areas that experienced misclassification, upon confirming with local experts from ISGS and NOAA, the results with the additional ROIs visually appeared to be most accurate and thus, the additional ROIs helped account for misclassified areas both in the nearshore and in cases of confusion between coarse unconsolidated and anthropogenic classes. However, the CA MNF FU with additional ROIs yielded an increase in pixels classified as fine unconsolidated in offshore areas following the flight line pattern (Figure 13, panel b), suggesting that the single data input was not sufficient for overcoming misclassifications even with additional training data. In general, classifications combining three or more of the airborne data inputs (except for CA MNF FU and CA MNF FU + CA MNF WLR) performed consistently and had overall accuracies of 90% or higher (KCs > 0.49). In addition, the use of spectral data inputs, CA MNF FU and WLR, was especially important for producing higher overall accuracies for the substrate component with 13 out of 15 data combinations including both spectral data inputs for combinations with overall accuracies of 90% or higher.

Classification results from the satellite data combinations generally showed the same substrate patterns as the airborne data combinations, except that anthropogenic features could not be resolved (Figure 14). The satellite data combinations with the highest overall classification accuracy included ones in which all three data inputs were used and in which either S2 MS or S2 DII was first in the data order. They included the following: S2 MS + S2 DII + S2 SDB (and two additional combinations using the same data but in a different order, S2 MS + S2 SDB + S2 DII and S2 DII + S2 SDB + S2 MS). Only one of the top-performing data combinations was further evaluated with additional ROIs since all had the same overall accuracy. Figure 14 illustrates the two Tier 1 substrate classification results without and with additional ROIs (panels a and b, respectively). Overall and class-specific accuracies remained unchanged due to a lack of ground truth available for validation in select areas (Table A1, Appendix A), yet the addition of ROIs helped to visibly reduce the misclassification of coarse unconsolidated substrate in the northeast offshore part of the study area and discriminate coarse unconsolidated substrate that was missed just south of the intake pipeline. Similar to Wicaksono et al. [22], the classification results using DII tended to be highest. Data order was generally not a factor; however, when S2 SDB was input first with S2 DII + S2 MS, it resulted in a slight decrease in overall accuracy and KC, which may suggest that the S2 SDB input data, the algorithms used to derive it, and the resulting outputs should warrant further investigation and evaluation, especially when used as input into benthic classifications or models (see Discussion Section 4 for additional evaluation of the S2 SDB product).

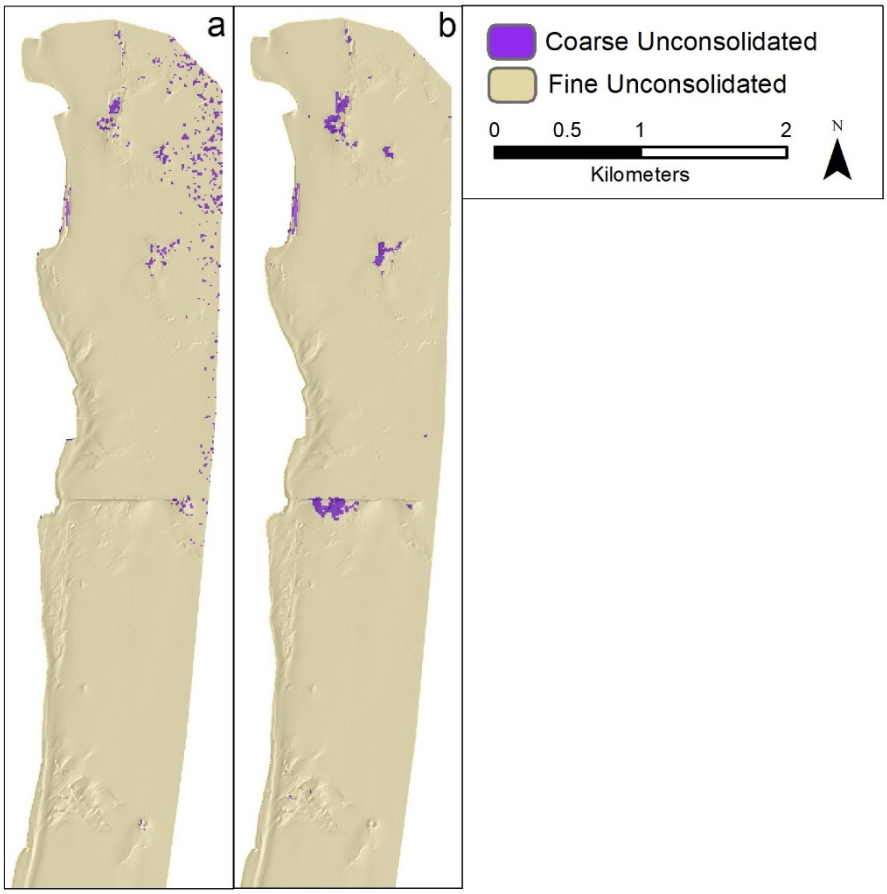

Figure 14. Tier 1 substrate component classification results using satellite data combinations for the north-central section of the study area: (**a**) S2 MS + S2 DII + S2 SDB and (**b**) S2 MS + S2 DII + S2 SDB with additional ROIs.

Tier 2 Substrate

For the Tier 2 fine unconsolidated (substrate) classification, overall accuracy (airborne only) was 93.28% for the two data combinations evaluated, while the KC was 0. The CA MNF FU data combination with additional ROIs, though considered one of the top-performing results, was unable to resolve any of the Tier 2 substrate classes. Therefore, the remaining top two data combinations were evaluated: (1) CA MNF WLR + CA MNF FU + AB DE with additional ROIs and (2) CA MNF FU + CA MNF WLR with additional ROIs. Since the CA MNF WLR + CA MNF FU + AB DE with additional ROIs data combination had the higher overall accuracy and KC of the two from Tier 1, the fine unconsolidated substrate area from that classification result was used as a mask to further discriminate more detailed (Tier 2) class types within that area. Although six sand classes with varying patterns (ripple and pockmarked surface patterns) and co-existing materials (woody debris, organic detritus, and mussel shell hash) were attempted with the SVM classifier, only two were able to be identified: (1) sand, and (2) sand with ripple surface pattern, with the majority of the sand with ripple surface pattern area located in the offshore, northeast part of the study area (Figure 15). Given a KC of 0 and no ground truth available for validation in that area, the reliability of the resultant classification is very low with this same classification result possible by chance. It is also worth mentioning that this location is in the same area where CA MNF FU with additional ROIs follows the flight line pattern (Figure 13, panel b). Thus, more detailed ground truth and data inputs would likely be needed to reliably classify the Tier 2 classes identified in this study, including the characterization of modifiers such as surface patterns or co-existing materials. Yet, it is worth noting that the classes listed in Tier 2 reflect the highest level of detail (subgroup level) within the substrate component of the CMECS hierarchy.

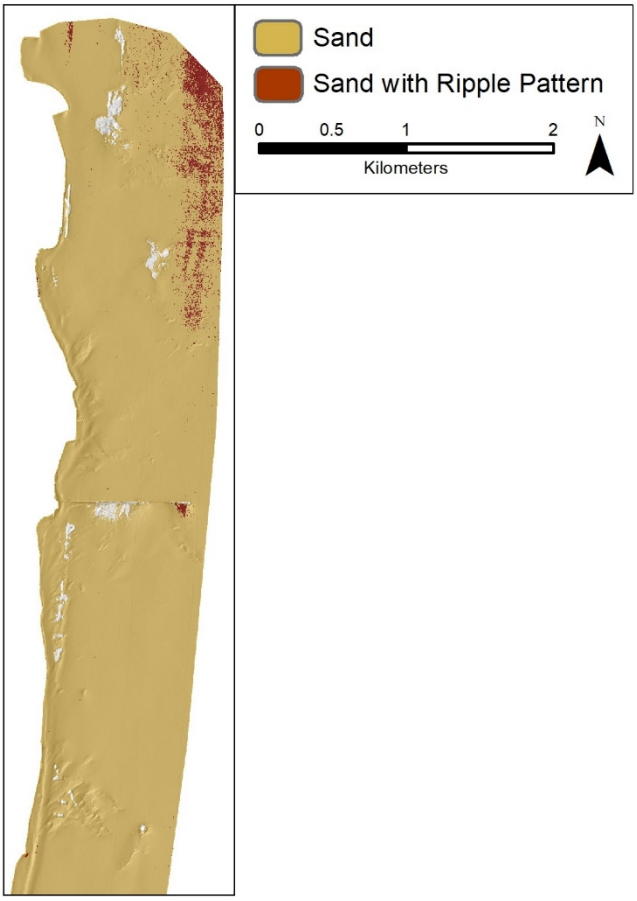

Figure 15. Tier 2 fine unconsolidated (substrate) classification results using airborne data combinations for the north-central section of the study area: CA MNF WLR + CA MNF FU + AB DE and CA MNF FU + CA MNF WLR.

3.1.2. Biotic Component Classification Results

Tier 1 Biotic

For the biotic component, average overall accuracy for the 24 airborne data combinations was 93.58 ± 0.91% (including data combinations with additional ROIs), while for the 11 satellite data combinations it was 92.67 ± 0.71% (data combinations with additional ROIs were not included). Similar to the results for the substrate component, KCs were more moderate to low, averaging 0.38 (±0.14) for airborne data combinations and 0.31 (±0.07) for satellite data combinations. Table A2 (Appendix A) lists the percent overall accuracy and KC, as well as the percent area and producer and user accuracies for the two classes (aquatic vegetation bed and biotic null) using airborne and satellite data combinations. As with the substrate component, the Index field in Table A2 (Appendix A) is a numerical value that is referenced in Figures 16 and 17 in which classification performance is plotted (percent overall accuracy compared to percent producer accuracy) to help illustrate patterns with respect to unique data combinations. Generally, the classifications showed that the majority of the area fell into the biotic null class with airborne data combinations estimating 97.42% (±1.26%) and satellite data combinations estimating a higher coverage amount of 98.33% (±1.13%). However, pockets of the aquatic vegetation bed class occurred largely coincident with the coarse unconsolidated substrate class in the central and northern parts of the study area with airborne data combinations estimating 2.58% (±1.26%) and satellite data combinations estimating a little less, 2.3% (±0.43) (Figure 18; Table A2, Appendix A).

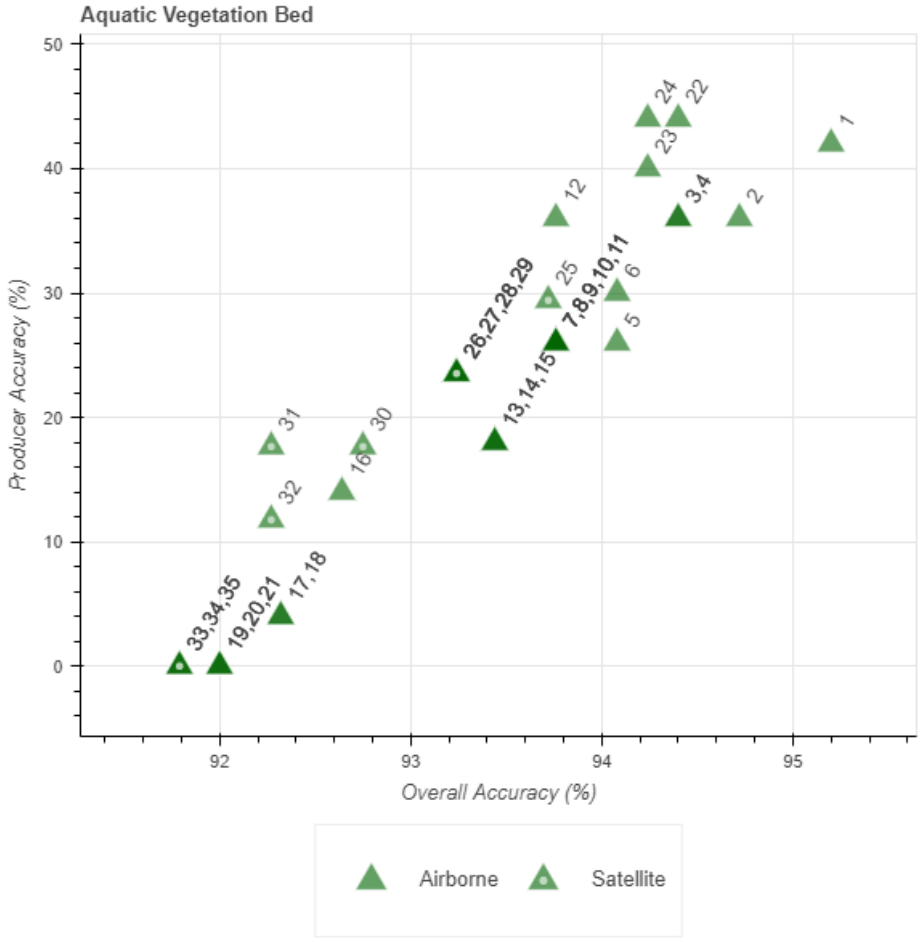

Figure 16. Tier 1 plot of aquatic vegetation bed classification performance, comparing percent overall accuracy and percent producer accuracy for airborne and satellite data combinations. Number labels refer to unique classification input data combinations identified in the Index field in Table A2, Appendix A.

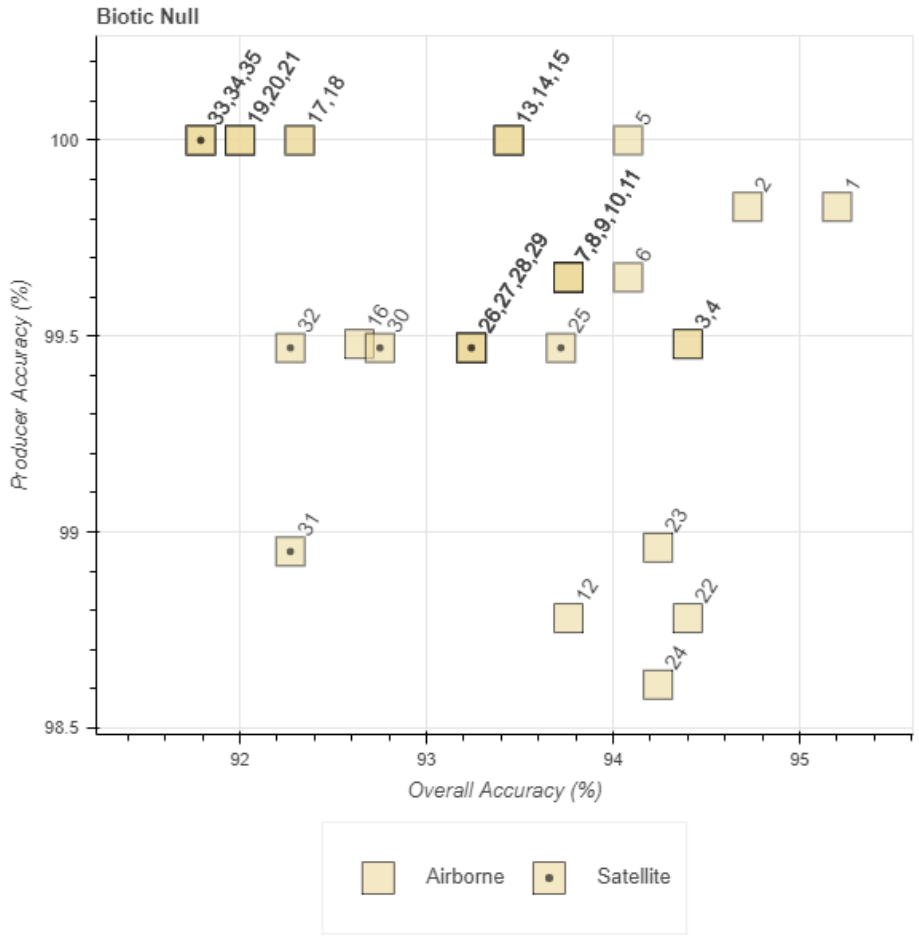

Figure 17. Tier 1 plot of biotic null classification performance, comparing percent overall accuracy and percent producer accuracy for airborne and satellite data combinations. Number labels refer to unique classification input data combinations identified in the Index field in Table A2, Appendix A.

The three airborne data combinations with the highest overall classification accuracies included the following (highest to lowest): (1) AB DE + CA MNF FU + CA MNF WLR, (2) CA MNF FU + CA MNF WLR, and (3) AB RF + AB DE + CA MNF FU + CA MNF WLR. These top three data combinations with additional ROIs were also evaluated for accuracy performance. Figure 18 illustrates the six top results for the Tier 1 biotic component. All three classification results using original ROIs tended to misclassify the aquatic vegetation bed class along the immediate shoreline (Figure 18, panels a, c and e). This was likely due to a lack of ground truth available in that part of the study area, and thus, when additional ROIs were added, the classification errors were corrected and likewise resulted in increased aquatic vegetation bed in areas coinciding with coarse unconsolidated substrate where it is known to occur (Figure 18, panels b, d and f). In fact, all classification results using original ROIs generally tended to underestimate the overall amount of the aquatic vegetation bed class in the study area (despite the overclassification along the immediate shoreline), averaging approximately 2.26% (±1.03%) as opposed to 4.53% (±0.33%) with additional ROIs. As with the substrate component, the spectral data inputs played an important role in the classification of the biotic component. However, the data combination with the highest overall accuracy and KC had AB DE as first in combination with spectral data inputs, suggesting that for aquatic vegetation bed discrimination that depth (fused with spectral data) could be more influential than one data type alone [51]. In contrast, when AB RF was added to the combination, while still among the top performers when used in combination with the other data inputs and used first, the overall accuracy and KC decreased (−0.8%, −0.08, respectively). Unlike the substrate component, there was not

an evident grouping of data combinations that performed as consistently for the biotic component, and KCs fell below 0.48 beyond the top four data combinations (Figure 16; Table A2, Appendix A).

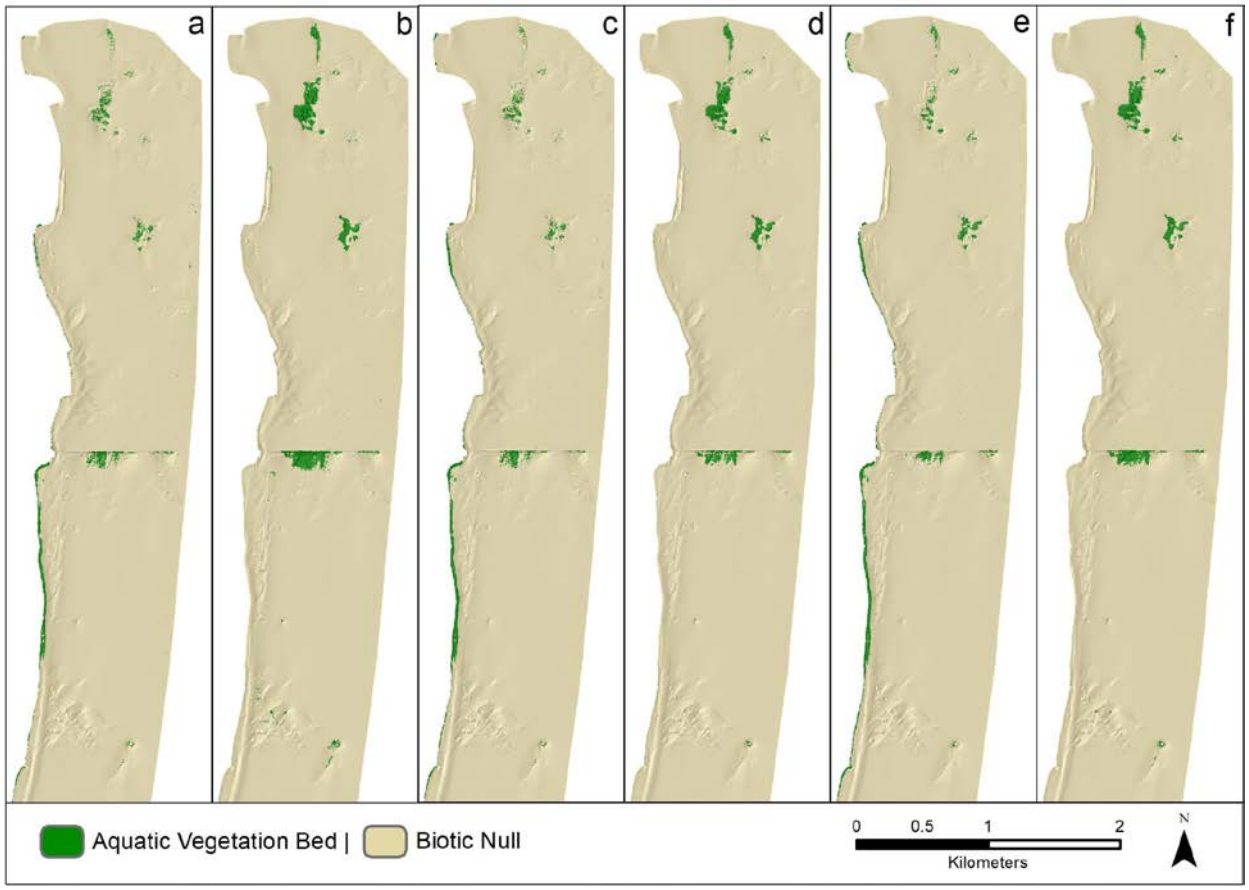

Figure 18. Tier 1 biotic component classification results using airborne data combinations for the north-central section of the study area: (**a**) AB DE + CA MNF FU + CA MNF WLR, (**b**) AB DE + CA MNF FU + CA MNF WLR with additional ROIs, (**c**) CA MNF FU + CA MNF WLR, (**d**) CA MNF FU + CA MNF WLR with additional ROIs, (**e**) AB RF + AB DE + CA MNF FU + CA MNF WLR, and (**f**) AB RF + AB DE + CA MNF FU + CA MNF WLR with additional ROIs.

Classification results from the satellite data combinations generally showed the same biotic component Tier 1 class patterns; however, obvious misclassifications were observed especially in the offshore, northeast section of the study area (Figure 19). The satellite data combinations with the highest overall classification accuracy included the following (highest to lowest): (1) S2 MS + S2 DII + S2 SDB, (2) S2 MS + S2 DII (and reverse order), and (3) S2 SDB + S2 DII + S2 MS (and one additional combination using the same data but in a different order, S2 DII + S2 SDB + S2 MS). No performance accuracies were evaluated with additional ROIs since attempted additions were unsuccessful in resolving misclassifications. Figure 19 illustrates the top three Tier 1 results for the biotic component using satellite data combinations. As with the substrate component, the top-performing data combination was S2 MS + S2 DII + S2 SDB; however, data order suggested a more influential role in the discrimination of classes in the biotic component (Figure 16). For example, when either S2 SDB or S2 DII was input ahead of S2 MS, overall accuracy and KC slightly decreased (−0.48%, −0.07, respectively). Additionally, the order of S2 DII and S2 SDB following S2 MS likewise impacted results and reduced overall accuracy and KC by −1.45% and 0.17, respectively. Regardless, obvious misclassifications could not be corrected, and as with the substrate component, the classification results using DII tended to be highest.

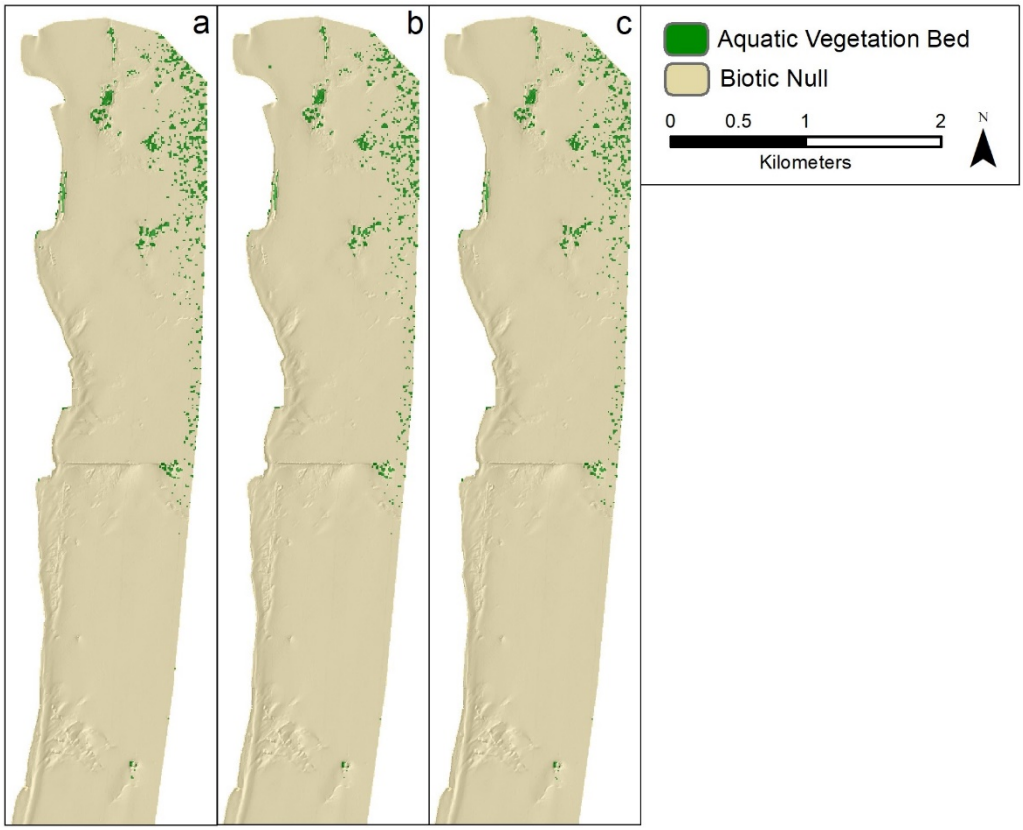

Figure 19. Tier 1 biotic component classification results using satellite data combinations for the north-central section of the study area: (**a**) S2 MS + S2 DII + S2 SDB, (**b**) S2 MS + S2 DII, and (**c**) S2 SDB + S2 DII + S2 MS.

Tier 2 Biotic

For the Tier 2 aquatic vegetation bed (biotic) classification, overall accuracy (airborne only) was 95.25% for the three data combinations evaluated and the KC was 0.86. The top three data combinations were evaluated: (1) AB DE + CA MNF FU + CA MNF WLR with additional ROIs, (2) CA MNF FU + CA MNF WLR with additional ROIs, and (3) AB RF + AB DE + CA MNF FU + CA MNF WLR with additional ROIs. Since the AB DE + CA MNF FU + CA MNF WLR with additional ROIs data combination had the highest overall accuracy and KC of the three from Tier 1, the aquatic vegetation bed area from that classification result was used as a mask to further discriminate more detailed (Tier 2) class types within that area. Two classes were identified: (1) *Cladophora* sp. and (2) *Cladophora* sp. with co-existing attached mussels (Figure 20). Unlike the Tier 2 fine unconsolidated (substrate) classification, the Tier 2 aquatic vegetation bed (biotic) classification performed very well with a strong KC, suggesting that for this study, the airborne data inputs were reliable enough to discriminate the most detailed biotic communities in the CMECs hierarchy, including co-existing attached mussels.

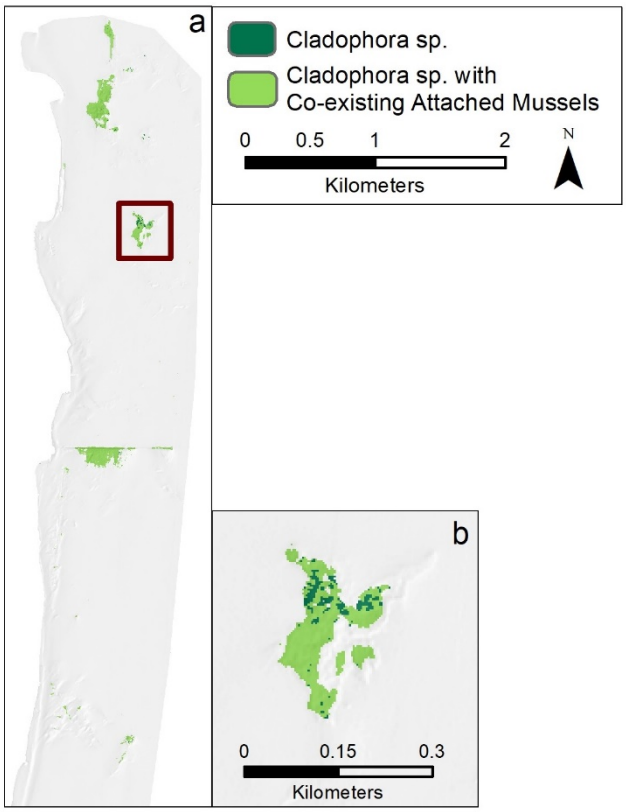

Figure 20. Tier 2 aquatic vegetation bed (biotic) classification results using airborne data combinations for the north-central section of the study area: (**a**) AB DE + CA MNF FU + CA MNF WLR, CA MNF FU + CA MNF WLR, and AB RF + AB DE + CA MNF FU + CA MNF WLR) and (**b**) inset panel corresponding to box in panel (**a**).

3.2. Component Classification Comparison

In addition to comparisons made between data types and tiered classes within components, comparisons were also possible between the components themselves. This provides a better understanding of the potential strengths and weaknesses of classification approaches and data types related to the substrate and biotic components. Such a comparison further illustrates which components may better lend themselves to classification depending upon the data types used in the analysis as well as provide insight into the methods that work best for each one or where improvement and further investigation may be needed.

In general, overall classification accuracies were higher for the biotic component than for the substrate component, regardless of data type (airborne vs. satellite) (Figure 21; Tables A1 and A2). More specifically, the biotic component classifications had higher average overall accuracies of 3.48% for airborne data combinations and 2.9% for satellite data combinations. This may be due in part to the additional class complexity involved with the Tier 1 substrate component which had three classes, including coarse unconsolidated and anthropogenic classes that could have spectrally similar materials (i.e., concrete) and lead to potential classification confusion. In contrast, the biotic component had lower average KCs by 0.09 for airborne data combinations, while they remained approximately the same between components for satellite data combinations. Yet, for airborne data combinations, the biotic component had greater variability among KCs ($\pm$0.14) as opposed to the substrate component ($\pm$0.08), while the top-performing airborne data combinations for the biotic component had KCs on par with the top-performing satellite data combinations for the substrate component (~0.55).

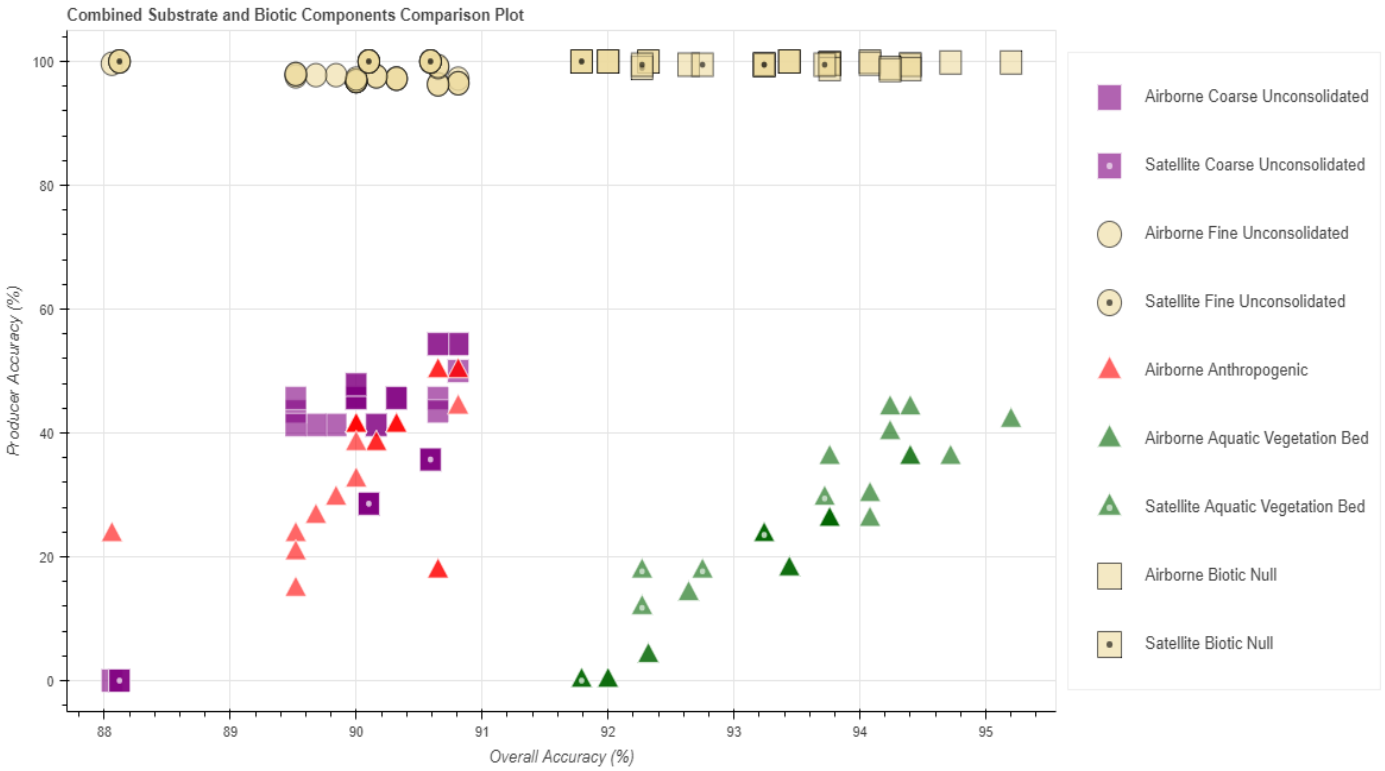

Figure 21. Tier 1 plot of substrate and biotic components classification performance, comparing percent overall accuracy and percent producer accuracy for airborne and satellite data combinations. Note the strong break in overall accuracy between substrate and biotic components and producer accuracy between the larger homogeneous components of the study area.

Regarding data types, the satellite data combinations with the highest accuracies were somewhat consistent between components, and the best results for substrate and biotic classifications included all three three data types: S2 MS + S2 DII + S2 SDB. However, there were some small variations between components, reflecting the impact of changes in data input order. For example, the substrate component appeared to be less influenced by the data input order, whereby S2 MS + S2 SDB + S2 DII and S2 DII + S2 SDB + S2 MS resulted in the same accuracies as the top performer. It was only when S2 SDB was used first in the data order that it resulted in a slight accuracy decrease. In contrast, the biotic component appeared a little more sensitive to data input order in which S2 SDB + S2 DII + S2 MS and S2 DII + S2 SDB + S2 MS experienced a slight decrease in accuracy compared to the top performer, while S2 MS + S2 SDB + S2 DII experienced an additional accuracy decrease. Thus, S2 DII may play an important role for the biotic component relative to the other data inputs. A similar finding was also present in Wicaksono et al. [22] in which two out of three machine learning approaches evaluated performed best when DII was used in the classification and was especially helpful for separating biotic coral reef and seagrass classes.

For the airborne data combinations, there was less consistency between components in terms of data inputs, but both components had top performers with the data combination: CA MNF FU + CA MNF WLR. This speaks to the dominant role of spectral information from the hyperspectral imagery and is consistent with similar approaches [23]; however, what is less clear, and not evaluated as part of this study, is the impact of dimensionality reduction techniques applied to the hyperspectral imagery (such as MNF or principal component analysis), which has had mixed results in terms of classification accuracy in other studies [22]. Additionally, out of the top five performing airborne data combinations for the substrate component, two included depth with spectral data inputs, though the inclusion of depth resulted in a slight accuracy decrease. In contrast, depth and bathymetric

reflectance data inputs were present in the top-performing data combinations for the biotic component, such as AB DE + CA MNF FU + CA MNF WLR and AB RF + AB DE + CA MNF FU + CA MNF WLR. This suggests an important role for the addition of Lidar-based data inputs for the classification of biotic classes, although this is somewhat mixed for other studies [22,23,52], and yet [22] acknowledges that the quality of the bathymetry data is likely the limiting factor. The CMECS structure used herein allowed for a more thorough review of the influence upon classification accuracy with respect to the component, whereas other studies tend to develop an inclusive classification system in which substrate classes (i.e., rock, sand, etc.) and biotic classes (i.e., seagrass, algae, etc.) are analyzed simultaneously. As a result, inclusive classification systems can make it difficult to understand the influence of data type on classification accuracy.

4. Discussion

The overall goal of this effort was to better understand airborne and satellite data inputs for identifying and classifying nearshore benthic substrate and associated habitat using a machine learning approach that could be easily repeated and applied in other shallow coastal environments. The study builds on foundational efforts to move towards a more integrated data approach, whereby data strengths and limitations for mapping nearshore benthic substrate and associated habitat, expressed through classification accuracy, were evaluated within the context of the CMECS classification hierarchy. The tiered approach allowed for iterative classification into higher levels of CMECS class detail in order to establish a "point of no return" or classification limit for data inputs, revealing which datasets are best suited for detecting substrate and biotic features at varying levels of specificity. This is important as we learn how to best piece different types of data together to create a regional picture at project-relevant resolutions, making sure to place them where they fit best and thus, matching end-goals or requirements with suitable data inputs in a strategic way. In that sense, various data inputs can be integrated in a complementary way to address a range of management or restoration needs, which is similar to a multi-sensor approach for restoration monitoring recommended for terrestrial applications suggested in Reif and Theel [53]. Yet, benthic mapping poses additional challenges that makes basin-wide or regional mapping more difficult than in terrestrial applications.

One of these challenges is the lack of a consistent classification system for benthic mapping applications, making it difficult to compare results from existing studies, and thus leading to further difficulties with advancing associated technical methods. Wicaksono et al. [22] touches on this issue explaining that there was difficulty comparing their results to others due to the uniqueness of the employed classification systems. Regardless, attempts to compare results in a general sense were made, and for this study, although the system used in Wicaksono et al. [22] had 13 classes combining substrate and biotic features using SVM applied to high-resolution satellite imagery, our overall accuracy was higher (by as much as 15% for substrate and 19% for biotic components), which is not surprising given the fewer number of classes in our study. Other machine learning techniques evaluated in Zhang et al. [23] with hyperspectral data fusion using OBIA and resulting in uniquely developed 3- and 9-class habitat maps had overall accuracies that were closer to the ones achieved in our study, 88.5% and 83.25%, respectively, though their KCs tended to be higher compared to our Tier 1 values, averaging 0.75 and 0.72, respectively. Alternatively, Marcello et al. [49] applied SVM (among other approaches) to airborne hyperspectral imagery as well as high-resolution satellite imagery in combination with in situ measurements from ship-based transects to identify 3 classes (2 substrate and 1 biotic) in a shallow coastal environment and, similar to our study, found that SVM applied to airborne hyperspectral imagery resulted in the highest overall accuracy; however, their range in overall accuracy using airborne data inputs was greater (73.33–97.36%, averaging 88.69%) and as much as ~2% higher than our highest overall accuracy.

Despite generalized comparisons, without a consistent, standard classification system, such as in wetland and other habitats, evaluation and establishment of best practices with

respect to data collection, processing, and analysis are hampered. The dissimilarity between benthic environments is noted in Wicaksono et al. [22] and thus, specific or complex classification systems cannot be applied to other areas. Furthermore, Kutser et al. [7] states that coastal variability precludes a consistent system, especially given that most systems are driven by optical signatures which often do not align with classes requested by coastal managers. However, CMECS may overcome these issues and offers a flexible solution that would not only increase opportunities for comparative studies, but also, expand exploration of methodological portability, which is one of the primary needs for advancing the state-of-the-science surrounding benthic mapping. Furthermore, CMECS' hierarchical structure ensures a level of flexibility and customization that likewise satisfies wide-ranging coastal management needs while striking a balance with ease of application—another point raised in Wicaksono et al. [22]. Another benefit of a standardized, hierarchical system is that it is data type- and sensor-agnostic meaning that it can be applied to any data, including from field observations as well as active or passive remote sensing. Additionally, while this study explores the implications for data types to resolve various levels within the CMECS hierarchy, such seamless system implementation would be a big step forward in benthic mapping research and toward the overall goal for basin-wide mapping.

Another challenge in nearshore coastal benthic mapping includes the need for more frequent, high-resolution bathymetry data, and thus, there is an increased opportunity for modeled data such as SDB to supplement airborne and vessel-based data collection. The Sentinel-2 satellite specifically offers advantages for deriving SDB and benthic habitat classification, owing to the 10–20 m spatial resolution, 5-day revisit cycle allowing rapid response mapping, coastal aerosol band, and free, open data access [10,54]. While there is increased use of SDB in benthic mapping applications, the implications of the data usage to coastal zone management and decision making remains unclear, especially considering varying spatial scales of projects. Recent evaluations of SDB algorithms (e.g., Lyzenga, Stumpf, Traganos, and Dierssen) using Sentinel-2 imagery within Google Earth Engine showed a wide range of root mean square error (RMSE) when modeled data were compared to in situ measurements from a single-beam echosounder with the highest accuracy resulting in an RMSE of 1.67 m, explaining 90% of the variation in the validation dataset [55]. A similar validation assessment was conducted in our study area in which bathymetry points from the airborne bathymetric lidar point cloud (30 cm vertical accuracy) were used to validate the modeled SDB, resulting in an RMSE of 1.02 m, explaining 76% of the variation in the validation dataset (Figure 22). The map in Figure 23 illustrates the tendency for the SDB to overestimate depths offshore (making it appear deeper) as opposed to underestimate depths nearshore (making it appear shallower). This trend also happens to coincide with areas that were prone to misclassification, such as the northeast section of the study area with optically deeper water and may exacerbate or confound classification issues associated with particular features or in certain areas. While this study utilized the algorithms associated with Sen2Coral process, it is understood that there are additional SDB inputs and algorithms available that could be evaluated and may provide better results; however, the comparison of these methods was not the focus of this study. Thus, it's important to understand how these data can impact not only the products resulting from their analytical use, but also the use of those resultant products in decision making, such as better understanding habitat changes pre- and post-placement of in-water shoreline protection structures, impacts to known fish spawning grounds (e.g., littoral sedimentation at Buffalo Reef in Lake Superior [28]), and the relationship between invasive species and changes to the benthic community at Sleeping Bear Dunes in Lake Michigan. Supplemental or tangential analyses such as the one presented in Figures 22 and 23, comparing SDB to high-fidelity in situ measurements or high-accuracy bathymetric lidar data, helps to better understand SDB accuracy in conjunction with benthic classification outputs and in relation to locally specific coastal management activities.

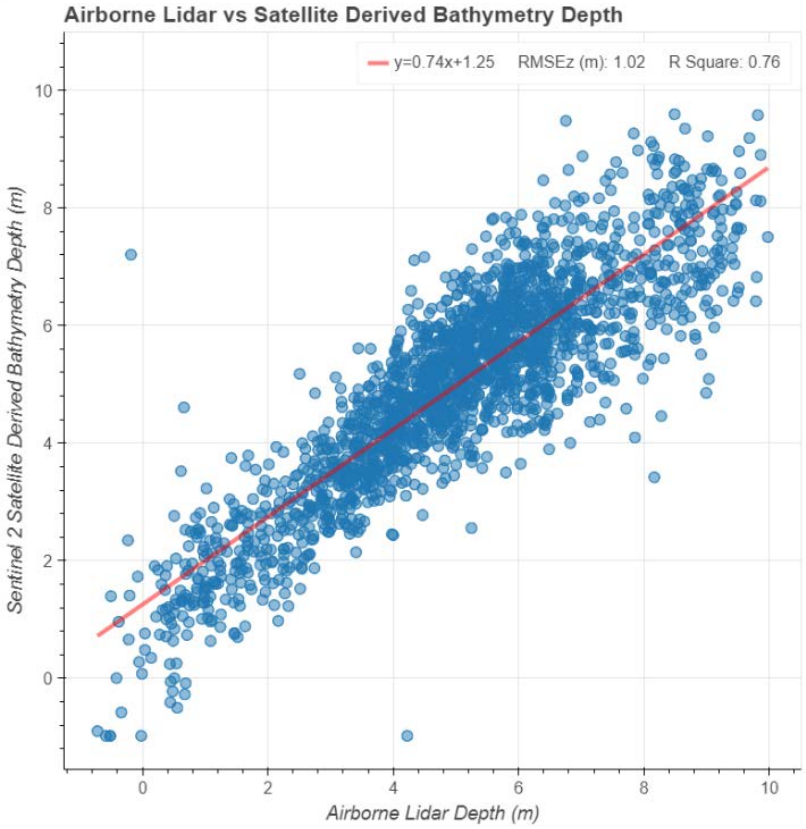

Figure 22. Plot comparison of SDB generated from Sentinel-2 imagery to airborne bathymetric lidar point cloud (30 cm vertical accuracy).

Other challenges specific to the progress in benthic mapping stem from the variety and increasing amounts of in situ observations, yet this also poses a tremendous opportunity, especially for moving towards semi-automation and machine learning approaches that rely on extensive ground verification data. To that end, the use of machine learning techniques for benthic mapping is a growing area of study with many documented benefits despite the tradeoffs associated with computation time and added ground validation requirements [7,21–23,56]. Ultimately, a compromise is needed to balance the desire for basin-wide, regionally consistent map products and the requirement for improved and increasing amounts of ground validation or ground truth data to satisfy machine learning and more automated approaches. In this study, the partnership with local experts was critical for gaining a priori knowledge to improve classification results. For example, without the cultural context of the shoreline impacts specific to the study area (Figure 24), which were provided in the ground validation data and captured within the CMECS hierarchy, the anthropogenic features identified offshore could have easily been identified as geologic coarse substrate given the spectrally similarity and shape of the materials. Figure 24 offers a historical perspective of changes in this highly dynamic area further illustrating how the data used in this study in combination with high-quality ground truth data and local knowledge can be used to monitor specific changes that have direct implications for natural resource policy-making and to inform restoration practices. Thus, it is important to think about strategic integration and application of the increasing amounts of field observations made by academia, state, local, and federal agencies, as well as many stakeholder and partner organizations to improve basin-wide mapping approaches. This ties back to the need for more consistent or standardized classification systems, in which CMECS may offer a consistent and flexible way for the application of field observation data. Wicaksono et al. [22] posits that in situ training or ground data are no longer necessary, which may be true in large homogeneous environments or areas with common benthic

features. However, in the case of the Great Lakes, there is a wide variety in nearshore substrate and biotic compositions in which the incorporation of field observations is essential for the development of accurate and reliable benthic habitat information and mapping products to support coastal and natural resources management.

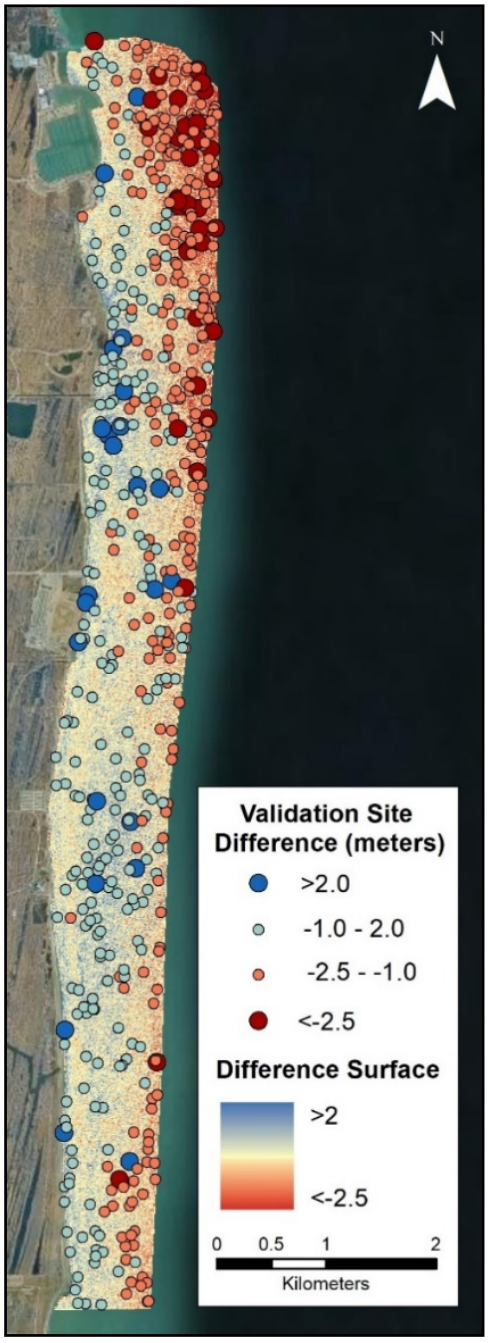

Figure 23. Map comparison of SDB generated from Sentinel-2 imagery to airborne bathymetric lidar point cloud (30 cm vertical accuracy), highlighting the tendency for the SDB to overestimate depths offshore (red sites, making it appear deeper) as opposed to underestimate depths nearshore (blue sites, making it appear shallower). Note that validation points within the RMSE range of $\pm$1.02 m were removed from the map graphic.

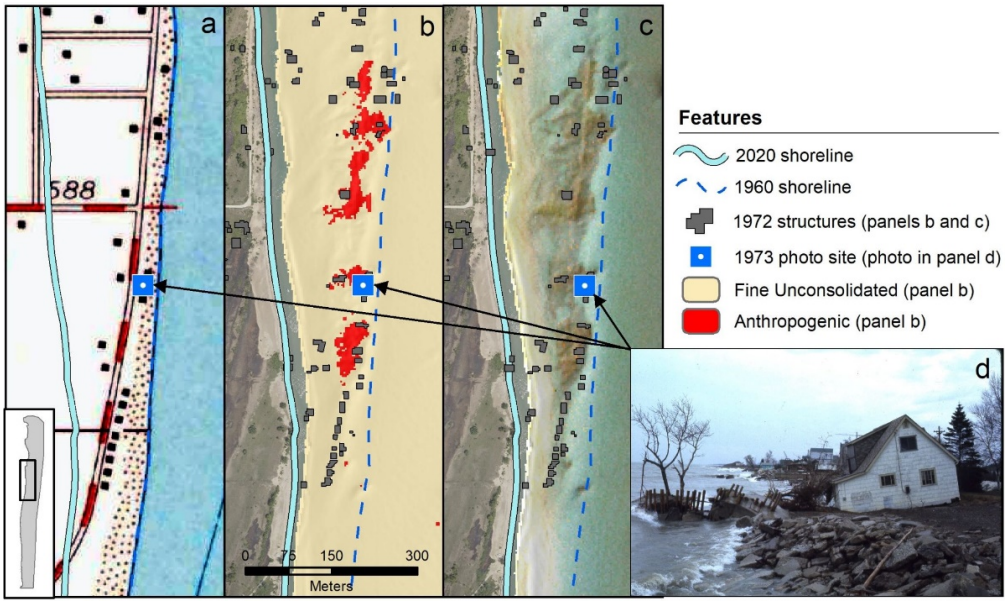

Figure 24. Shoreline changes and destruction of infrastructure illustrated in the central part of the study area as a result of lake level changes between 1960 and 2020: (**a**) 1960 topographic map obtained from the U.S. Geological Survey [57] showing homes and roads along the shoreline with the superimposed 2020 shoreline (digitized from RGB aerial imagery collected by the JALBTCX in 2020), (**b**) Tier 1 substrate classification result using airborne data inputs from 17 July 2018, highlighting remnants of various infrastructure found offshore (1973 structures digitized from historic topographic maps, [58]) and classified as anthropogenic substrate (in red), (**c**) airborne fusion image from 17 July 2018 also illustrating offshore benthic environment, and (**d**) 1973 photograph showing destruction of a home impacted by the shoreline erosion [59].

5. Conclusions

The approach described in this study, in which airborne and satellite data were evaluated for the classification of benthic substrate and biotic components reveals the potential strengths and weaknesses of those datasets for use in basin-wide mapping. Furthermore, it shows how these different approaches can be complementary, revealing levels of certainty when used in tandem or if fused or integrated more directly. This integrative aspect is important as regional initiatives such as the Great Lakes Water Quality Agreement strive to find ways to better protect and restore aquatic resources, in which monitoring and adaptive management are key objectives, setting the stage for critical regional activities and policies [4]. For example, the products generated from this study could be used to better understand the benthic substrate and associated habitat prior to shoreline protection project implementation (pre- and post-placement of shoreline protection structures) funded by the Great Lakes Restoration Initiative.

Future steps should include not only evaluating the portability of the approach developed in this study to other areas in the Great Lakes, but also further integrating additional data types, such as vessel-based measurements, at larger spatial extents. Scaling analytical efforts up will increase the class diversity and complexity as well as require bringing even more disparate data types together, a challenging endeavor. Yet, no single data type or platform can accomplish the goal of basin-wide nearshore benthic mapping, and given the high variability of the nearshore environment within the Great Lakes, a multi-sensor data integration approach is warranted. A large piece of the regional puzzle will include the integration of airborne and satellite data, and many of the previous hurdles surrounding their use continue to improve—higher spatial, spectral, and temporal resolutions, better data quality, enhanced water column correction techniques, more advanced analytical methods, such as machine learning, as well as free, open data policies. Coastal and nearshore mapping programs and initiatives including the USACE NCMP, Seabed 2030, and Lakebed

2030, to name only a few of the efforts underway, are working to increase the temporal and spatial resolution of available data. It will be important to scale the benthic mapping work accordingly to take advantage of these new data streams and create meaningful, accurate, and reliable benthic data products that support the coastal and natural resources management professionals. The nexus of these technical improvements, along with a flexible classification system that meets management needs while being widely applicable (e.g., CMECS), and cross-jurisdictional partnerships for leveraging data, expertise, and resources will ultimately help overcome the challenges associated with basin-wide nearshore benthic mapping.

Author Contributions: Conceptualization, M.K.R. and B.S.K.; methodology, M.K.R., B.S.K., S.E.B. and E.J.T.; software, M.K.R., B.S.K. and J.H.H.; validation, M.K.R., B.S.K., S.E.B. and E.J.T.; formal analysis, M.K.R. and B.S.K.; investigation, M.K.R., B.S.K. and J.H.H.; resources, M.K.R., B.S.K., S.E.B. and E.J.T.; data curation, M.K.R., B.S.K., S.E.B., E.J.T. and J.H.H.; writing—original draft preparation, M.K.R.; writing—review and editing, M.K.R., B.S.K., S.E.B., E.J.T. and J.H.H.; visualization, M.K.R., B.S.K. and S.E.B.; supervision, M.K.R.; project administration, M.K.R.; funding acquisition, M.K.R., B.S.K., S.E.B. and E.J.T. All authors have read and agreed to the published version of the manuscript.

Funding: This research was funded by the U.S. Army Corps of Engineers, Engineer Research and Development Center's Ecosystem Management and Restoration Research Program, Vicksburg, Mississippi, USA. In situ data collections were funded in part through the Great Lakes Restoration Initiative in support of the Sustainable Nearshore Management Solutions to Prevent Critical Habitat Loss at Illinois Beach State Park project. Part of this study was funded by the Illinois Department of Natural Resources Coastal Management Program through a federal grant from NOAA, U.S. Department of Commerce.

Data Availability Statement: Airborne imagery and lidar data are publicly available and were obtained from the U.S. Army Corps of Engineers National Coastal Mapping Program. Final data products generated for this study are available by request from the corresponding author, Molly Reif (molly.k.reif@usace.army.mil).

Acknowledgments: The authors would like to thank Mark Finkbeiner from the National Oceanic and Atmospheric Administration's Office for Coastal Management for his assistance with and guidance for applying the Coastal and Marine Ecological Classification Standard (CMECS).

Conflicts of Interest: The authors declare no conflict of interest. Views, opinions, and/or findings contained herein are those of the authors and should not be construed as an official Department of the Army or the National Oceanic and Atmospheric Administration position or decision unless so designated by other official documentation.

Appendix A. Tier 1 Substrate and Biotic Component Classification Accuracy

Table A1. Tier 1 substrate component overall and class-specific classification accuracies for airborne and satellite data combinations. Index = unique numerical value; OA% = percent overall accuracy; KC = Kappa Coefficient; Area% = percent area; PA% = percent producer accuracy; UA% = percent user accuracy. Data combinations are ranked by overall accuracy, highest to lowest, and grouped in which overall accuracy and Kappa Coefficient values are the same (alternating groups of white, light grey and dark grey blocks); there is no particular order of importance within those groups. * Denotes the data combination used for the Tier 2 analysis mask.

				Coarse Unconsolidated			Fine Unconsolidated			Anthropogenic		
Index	**Data Type**	**OA%**	**KC**	**Area%**	**PA%**	**UA%**	**Area%**	**PA%**	**UA%**	**Area%**	**PA%**	**UA%**
	Airborne Data Combinations											
1	CA MNF FU	90.81	0.54	5.32	50	69.7	91.45	97.22	92.59	3.23	44.12	75
2	CA MNF FU + CA MNF WLR	90.81	0.56	5.65	54.35	71.43	90.16	96.48	93.2	4.19	50	65.38
3	CA MNF WLR + CA MNF FU	90.81	0.56	5.65	54.35	71.43	90.16	96.48	93.2	4.19	50	65.38
4	CA MNF WLR + CA MNF FU + AB DE	90.65	0.55	5.65	54.35	71.43	90	96.3	93.19	4.35	50	62.96
5	AB DE + CA MNF FU + CA MNF WLR	90.65	0.55	5.65	54.35	71.43	90	96.3	93.19	4.35	50	62.96
6	CA MNF FU + CA MNF WLR + AB RF	90.32	0.50	4.52	45.65	75	91.94	97.22	92.11	3.55	41.18	63.64

Table A1. *Cont.*

Index	Data Type	OA%	KC	Coarse Unconsolidated			Fine Unconsolidated			Anthropogenic		
				Area%	PA%	UA%	Area%	PA%	UA%	Area%	PA%	UA%
7	CA MNF WLR + CA MNF FU + AB RF	90.32	0.50	4.52	45.65	75	91.94	97.22	92.11	3.55	41.18	63.64
8	CA MNF FU + AB RF + CA MNF WLR	90.32	0.50	4.52	45.65	75	91.94	97.22	92.11	3.55	41.18	63.64
9	AB RF + CA MNF FU + CA MNF WLR	90.16	0.48	4.19	41.3	73.08	92.74	97.59	91.65	3.06	38.24	68.42
10	AB RF + AB DE + CA MNF FU + CA MNF WLR	90.16	0.48	4.19	41.3	73.08	92.74	97.59	91.65	3.06	38.24	68.42
11	CA MNF FU + CA MNF WLR + AB DE + AB RF	90.00	0.49	4.68	45.65	72.41	91.61	96.85	92.08	3.71	41.18	60.87
12	CA MNF WLR + CA MNF FU + AB DE + AB RF	90.00	0.49	4.68	45.65	72.41	91.61	96.85	92.08	3.71	41.18	60.87
13	AB DE + AB RF + CA MNF FU + CA MNF WLR	90.00	0.49	4.68	45.65	72.41	91.61	96.85	92.08	3.71	41.18	60.87
14	CA MNF FU + AB RF + AB DE + CA MNF WLR	90.00	0.49	4.68	45.65	72.41	91.61	96.85	92.08	3.71	41.18	60.87
15	CA MNF FU + AB DE + AB RF	90.00	0.49	4.84	47.83	73.33	91.61	96.85	92.08	3.55	38.24	59.09
16	CA MNF FU + AB RF	90.00	0.48	5	47.83	70.97	92.26	97.22	91.78	2.74	32.35	64.71
17	AB RF + AB DE + CA MNF FU	89.84	0.44	4.19	41.3	73.08	93.39	97.78	91.19	2.42	29.41	66.67
18	AB RF + CA MNF FU	89.68	0.43	4.19	41.3	73.08	93.55	97.78	91.03	2.23	26.47	64.29
19	AB DE + AB RF	89.52	0.42	4.52	43.48	71.43	93.39	97.59	91.02	2.1	23.53	61.54
20	AB RF + AB DE	89.52	0.41	3.87	41.3	79.17	94.03	97.96	90.74	2.1	20.59	53.85
21	CA MNF WLR	88.06	0.16	0	0	0	98.39	99.63	88.2	1.61	23.53	80
	Airborne Data Combinations with Additional ROIs											
22	CA MNF FU	90.65	0.45	4.19	45.65	80.77	94.84	99.07	90.99	0.97	17.65	100
23	CA MNF WLR + CA MNF FU + AB DE *	90.65	0.44	3.87	43.48	83.33	95.16	99.26	90.85	0.97	17.65	100
24	CA MNF FU + CA MNF WLR	89.52	0.41	4.52	45.65	75	94.03	97.96	90.74	1.45	14.71	55.56
	Satellite Data Combinations											
25	S2 MS + S2 DII + S2 SDB	90.59	0.32	2.48	35.71	100	97.52	100	90.36	n/a	n/a	n/a
26	S2 MS + S2 SDB + S2 DII	90.59	0.32	2.48	35.71	100	97.52	100	90.36	n/a	n/a	n/a
27	S2 DII + S2 SDB + S2 MS	90.59	0.32	2.48	35.71	100	97.52	100	90.36	n/a	n/a	n/a
28	S2 MS + S2 DII	90.10	0.27	1.98	28.57	100	98.02	100	89.9	n/a	n/a	n/a
29	S2 DII + S2 MS	90.10	0.27	1.98	28.57	100	98.02	100	89.9	n/a	n/a	n/a
30	S2 SDB + S2 DII + S2 MS	90.10	0.27	1.98	28.57	100	98.02	100	89.9	n/a	n/a	n/a
31	S2 DII + S2 SDB	90.10	0.27	1.98	28.57	100	98.02	100	89.9	n/a	n/a	n/a
32	S2 SDB + S2 DII	90.10	0.27	1.98	28.57	100	98.02	100	89.9	n/a	n/a	n/a
33	S2 MS	88.12	0	0	0	0	100	100	88.12	n/a	n/a	n/a
34	S2 MS + S2 SDB	88.12	0	0	0	0	100	100	88.12	n/a	n/a	n/a
35	S2 SDB + S2 MS	88.12	0	0	0	0	100	100	88.12	n/a	n/a	n/a
	Satellite Data Combinations with Additional ROIs											
36	S2 MS + S2 DII + S2 SDB	90.59	0.32	2.48	35.71	100	97.52	100	90.36	n/a	n/a	n/a

Table A2. Tier 1 biotic component overall and class-specific classification accuracies for airborne and satellite data combinations. Index = unique numerical value; OA% = percent overall accuracy; KC = Kappa Coefficient; Area% = percent area; PA% = percent producer accuracy; UA% = percent user accuracy. Data combinations are ranked by overall accuracy, highest to lowest, and grouped in which overall accuracy and Kappa Coefficient values are the same (alternating groups of white, light grey and dark grey blocks); there is no particular order of importance within those groups. * Denotes the data combination used for the Tier 2 analysis mask.

Index	Data Type	OA%	KC	Aquatic Vegetation Bed			Biotic Null		
				Area%	PA%	UA%	Area%	PA%	UA%
	Airborne Data Combinations								
1	AB DE + CA MNF FU + CA MNF WLR	95.2	0.56	3.52	42	95.45	96.48	99.83	95.19
2	CA MNF FU + CA MNF WLR	94.72	0.50	3.04	36	94.72	96.96	99.83	94.72
3	AB RF + AB DE + CA MNF FU + CA MNF WLR	94.4	0.48	3.36	36	85.71	96.64	99.48	94.7
4	AB RF + CA MNF FU + CA MNF WLR	94.4	0.48	3.36	36	85.74	96.64	99.48	94.7
5	CA MNF WLR + CA MNF FU	94.08	0.39	2.08	26	100	97.92	100	93.95
6	CA MNF WLR + CA MNF FU + AB DE	94.08	0.42	2.72	30	88.24	97.28	99.65	94.24
7	CA MNF WLR + CA MNF FU + AB DE + AB RF	93.76	0.38	2.4	26	86.67	97.6	99.65	93.93
8	CA MNF FU + CA MNF WLR + AB DE + AB RF	93.76	0.38	2.4	26	86.67	97.6	99.65	93.93
9	AB DE + AB RF + CA MNF FU + CA MNF WLR	93.76	0.38	2.4	26	86.67	97.6	99.65	93.93
10	CA MNF FU + AB RF + AB DE + CA MNF WLR	93.76	0.38	2.4	26	86.67	97.6	99.65	93.93
11	CA MNF FU + AB DE + AB RF	93.76	0.38	2.4	26	86.67	97.6	99.65	93.93
12	AB DE + AB RF	93.76	0.45	4	36	72	96	98.78	94.67
13	CA MNF WLR + CA MNF FU + AB RF	93.44	0.29	1.44	18	100	98.56	100	93.34
14	CA MNF FU + CA MNF WLR + AB RF	93.44	0.29	1.44	18	100	98.56	100	93.34
15	CA MNF FU + AB RF + CA MNF WLR	93.44	0.29	1.44	18	100	98.56	100	93.34
16	CA MNF FU	92.64	0.21	1.6	14	70	98.4	99.48	93.01
17	AB RF + AB DE + CA MNF FU	92.32	0.07	0.32	4	100	99.68	100	92.3
18	AB RF + AB DE	92.32	0.07	0.32	4	100	99.68	100	92.3
19	CA MNF WLR	92	0.00	0	0	0	100	100	92
20	CA MNF FU + AB RF	92	0.00	0	0	0	100	100	92
21	AB RF + CA MNF FU	92	0.00	0	0	0	100	100	92
	Airborne Data Combinations with Additional ROIs								
22	AB DE + CA MNF FU + CA MNF WLR *	94.4	0.53	4.64	44	75.86	95.36	98.78	95.3
23	AB RF + AB DE + CA MNF FU + CA MNF WLR	94.24	0.50	4.16	40	76.92	95.84	98.96	94.99
24	CA MNF FU + CA MNF WLR	94.24	0.52	4.8	44	73.33	95.2	98.61	95.29
	Satellite Data Combinations								
25	S2 MS + S2 DII + S2 SDB	93.72	0.41	2.9	29.41	83.33	97.1	99.47	94.03
26	S2 MS + S2 DII	93.24	0.34	2.42	23.53	80	97.58	99.47	93.56
27	S2 DII + S2 MS	93.24	0.34	2.42	23.53	80	97.58	99.47	93.56
28	S2 SDB + S2 DII + S2 MS	93.24	0.34	2.42	23.53	80	97.58	99.47	93.56
29	S2 DII + S2 SDB + S2 MS	93.24	0.34	2.42	23.53	80	97.58	99.47	93.56
30	S2 DII + S2 SDB	92.75	0.26	1.93	17.65	75	98.07	99.47	93.1
31	S2 MS + S2 SDB + S2 DII	92.27	0.24	2.42	17.65	60	97.58	98.95	93.07
32	S2 SDB + S2 DII	92.27	0.18	1.45	11.76	66.67	98.55	99.47	92.65
33	S2 MS	91.79	0	0	0	0	100	100	91.79
34	S2 MS + S2 SDB	91.79	0	0	0	0	100	100	91.79
35	S2 SDB + S2 MS	91.79	0	0	0	0	100	100	91.79

References

1. Lane, J.A.; Portt, C.B.; Minns, C.K. *Spawning Habitat Characteristics of Great Lakes Fishes*; Fisheries and Oceans Canada: Port Hardy, BC, Canada, 1996.
2. Burlakova, L.E.; Barbiero, R.P.; Karatayev, A.Y.; Daniel, S.E.; Hinchey, E.K.; Warren, G.J. The benthic community of the Laurentian Great Lakes: Analysis of spatial gradients and temporal trends from 1998 to 2014. *J. Great Lakes Res.* **2018**, *44*, 600–617. [CrossRef]
3. Madenjian, C.P.; Bunnell, D.B.; Warner, D.M.; Pothoven, S.A.; Fahnenstiel, G.L.; Nalepa, T.F.; Vanderploeg, H.A.; Tsehaye, I.; Claramunt, R.M.; Clark, R.D., Jr. Changes in the Lake Michigan food web following dreissenid mussel invasions: A synthesis. *J. Great Lakes Res.* **2015**, *40*, 217–231. [CrossRef]
4. Binational.Net. About the Great Lakes Water Quality Agreement. Available online: https://binational.net/glwqa-aqegl/ (accessed on 1 June 2021).

5. Menza, C.; Kendall, M.S.; Sautter, W.; Mabrouk, A.; Hile, S.D. Chapter 2: Lakebed Geomorphology, Substrates, and Habitats. In *Ecological Assessment of Wisconsin-Lake Michigan*; Menza, C., Kendall, M.S., Eds.; NOAA Technical Memorandum NOS NCCOS 257; NOAA NOS National Centers for Coastal Ocean Science, Marine Spatial Ecology Division: Silver Spring, MD, USA, 2019; pp. 5–30. [CrossRef]
6. Riseng, C.M.; Wehrly, K.E.; Wang, L.; Rutherford, E.S.; McKenna, J.E., Jr.; Johnson, L.B.; Mason, L.A.; Castiglione, C.; Hollenhorst, T.P.; Sparks-Jackson, B.L.; et al. Ecosystem classification and mapping of the Laurentian Great Lakes. *Can. J. Fish. Aquat. Sci.* **2018**, *75*, 1693–1712. [CrossRef]
7. Kutser, T.; Hedley, J.; Giardino, C.; Roelfsema, C.; Brando, V.E. Remote sensing of shallow waters—A 50 year retrospective and future directions. *Remote Sens. Environ.* **2020**, *240*, 111619. [CrossRef]
8. Wozencraft, J.M.; Dunkin, L.M.; Eisemann, E.R.; Reif, M.K. Applications, Ancillary Systems, and Fusion. In *Airborne Laser Hydrography II*; eCommons: Ithaca, NY, USA, 2019; pp. 207–230.
9. Reif, M.K.; Wozencraft, J.M.; Dunkin, L.M.; Sylvester, C.S.; Macon, C.L. A review of US Army Corps of Engineers airborne coastal mapping in the Great Lakes. *J. Great Lakes Res.* **2013**, *39*, 194–204. [CrossRef]
10. Bergsma, E.; Almar, R. Coastal coverage of ESA' Sentinel 2 mission. *Adv. Space Res.* **2020**, *65*, 2636–2644. [CrossRef]
11. Anderson, N.T.; Marchisio, G.B. WorldView-2 and the evolution of the DigitalGlobe remote sensing satellite constellation: Introductory paper for the special session on WorldView-2. In *Algorithms and Technologies for Multispectral, Hyperspectral, and Ultraspectral Imagery XVIII*; International Society for Optics and Photonics: Baltimore, MD, USA, 2012; Volume 8390. [CrossRef]
12. Vahtmäe, E.; Paavel, B.; Kutser, T. How much benthic information can be retrieved with hyperspectral sensor from the optically complex coastal waters? *J. Appl. Remote Sens.* **2020**, *14*, 16504. [CrossRef]
13. Stumpf, R.P.; Holderied, K.; Sinclair, M. Determination of water depth with high-resolution satellite imagery over variable bottom types. *Limnol. Oceanogr.* **2003**, *48*, 547–556. [CrossRef]
14. Eugenio, F.; Marcello, J.; Martin, J.; Rodríguez-Esparragón, D. Benthic Habitat Mapping Using Multispectral High-Resolution Imagery: Evaluation of Shallow Water Atmospheric Correction Techniques. *Sensors* **2017**, *17*, 2639. [CrossRef] [PubMed]
15. Brando, V.E.; Anstee, J.M.; Wettle, M.; Dekker, A.G.; Phinn, S.R.; Roelfsema, C. A physics based retrieval and quality assessment of bathymetry from suboptimal hyperspectral data. *Remote Sens. Environ.* **2009**, *113*, 755–770. [CrossRef]
16. Lee, Z.; Carder, K.L.; Mobley, C.D.; Steward, R.G.; Patch, J.S. Hyperspectral remote sensing for shallow waters: A semianalytical model. *Appl. Opt.* **1998**, *37*, 6329–6338. [CrossRef] [PubMed]
17. Kim, M.; Park, J.Y.; Aitken, J. Atmospheric correction of the CASI hyperspectral image using the scattering angle by the direct solar beam. In *Algorithms and Technologies for Multispectral, Hyperspectral, and Ultraspectral Imagery XVIII*; International Society for Optics and Photonics: Baltimore, MD, USA, 2012; Volume 8390. [CrossRef]
18. Garcia, R.A.; McKinna, L.I.W.; Hedley, J.D.; Fearns, P.R.C.S. Improving the optimization solution for a semi-analytical shallow water inversion model in the presence of spectrally correlated noise. *Limnol. Oceanogr. Methods* **2014**, *12*, 651–669. [CrossRef]
19. Casal, G.; Kutser, T.; Dominguez-Gomez, J.A.; Sanchez-Carnero, N.; Freire, J. Mapping benthic macroalgal communities in the coastal zone using CHRIS-PROBA mode 2 images. *Estuar. Coast. Shelf Sci.* **2011**, *94*, 281–290. [CrossRef]
20. Mumby, P.J.; Edwards, A.J. Mapping marine environments with IKONOS imagery: Enhanced spatial resolution can deliver greater thematic accuracy. *Remote Sens. Environ.* **2002**, *82*, 248–257. [CrossRef]
21. Mohamed, H.; Nadaoka, K.; Nakamura, T. Assessment of Machine Learning Algorithms for Automatic Benthic Cover Monitoring and Mapping Using Towed Underwater Video Camera and High-Resolution Satellite Images. *Remote Sens.* **2018**, *10*, 773. [CrossRef]
22. Wicaksono, P.; Lazuardi, W. Assessment of PlanetScope images for benthic habitat and seagrass species mapping in a complex optically shallow water environment. *Int. J. Remote Sens.* **2018**, *39*, 5739–5765. [CrossRef]
23. Zhang, C. Applying data fusion techniques for benthic habitat mapping and monitoring in a coral reef ecosystem. *ISPRS J. Photogram Remote Sens.* **2015**, *104*, 213–223. [CrossRef]
24. Diesing, M.; Green, S.L.; Stephens, D.; Lark, R.M.; Stewart, H.A.; Dove, D. Mapping seabed sediments: Comparison of manual, geostatistical, object-based image analysis and machine learning approaches. *Cont. Shelf Res.* **2014**, *84*, 107–119. [CrossRef]
25. Ierodiaconou, D.; Schimel, A.C.G.; Kennedy, D.; Monk, J.; Gaylard, G.; Young, M.; Diesing, M.; Rattray, A. Combining pixel and object based image analysis of ultra-high resolution multibeam bathymetry and backscatter for habitat mapping in shallow marine waters. *Mar. Geophys. Res.* **2018**, *39*, 271–288. [CrossRef]
26. Diesing, M.; Stephens, D. A multi-model ensemble approach to seabed mapping. *J. Sea Res.* **2015**, *100*, 62–69. [CrossRef]
27. Goetz, S.; Gardiner, N.; Viers, J. Monitoring freshwater, estuarine and near-shore benthic ecosystems with multi-sensor remote sensing: An introduction to the special issue. *Remote Sens. Environ.* **2008**, *112*, 3993–3995. [CrossRef]
28. Kerfoot, W.C.; Hobmeier, M.M.; Swain, G.; Regis, R.; Raman, V.K.; Brooks, C.N.; Grimm, A.; Cook, C.; Shuchman, R.; Reif, M. Coastal Remote Sensing: Merging Physical, Chemical, and Biological Data as Tailings Drift onto Buffalo Reef, Lake Superior. *Remote Sens.* **2021**, *13*, 2434. [CrossRef]
29. Rose, K.V.; Nayegandhi, A.; Moses, C.S.; Beavers, R.; Lavoie, D.; Brock, J.C. *Gap Analysis of Benthic Mapping at Three National Parks–Assateague Island National Seashore, Channel Islands National Parks, and Sleeping Bear Dunes National Lakeshore: U.S.*; US Geological Survey: Reston, VA, USA, 2012; p. 60.
30. McClinton, T. *Great Lakes Benthic Habitat Mapping: South Manitou Island Phase 2 CMECS Substrate and Biotic Components*; Technical report developed for NOAA Office for Coastal Management; David Evans and Associates: Vancouver, WA, USA, 2018; p. 32.

31. Menza, C.; Kendall, M.S. (Eds.) *Ecological Assessment of Wisconsin-Lake Michigan*; NOAA Technical Memorandum NOS NCCOS 257; NOAA NOS National Centers for Coastal Ocean Science, Marine Spatial Ecology Division: Silver Spring, MD, USA, 2019; p. 106. [CrossRef]
32. Shuchman, R.A.; Sayers, M.J.; Brooks, C.N. Mapping and monitoring the extent of submerged aquatic vegetation in the Laurentian Great Lakes with multi-scale satellite remote sensing. *J. Great Lakes Res.* **2013**, *39*, 78–89. [CrossRef]
33. Mwakanyamale, K.E.; Brown, S.E.; Theuerkauf, E.J. Delineating spatial distribution and thickness of unconsolidated sand along the southwest Lake Michigan shoreline using TEM and ERT geophysical methods. *J. Great Lakes Res.* **2020**, *46*, 1544–1558. [CrossRef]
34. Tuell, G.; Barbor, K.; Wozencraft, J. Overview of the coastal zone mapping and imaging lidar (CZMIL): A new multisensor airborne mapping system for the U.S. Army Corps of Engineers. *Proc. SPIE* **2010**, *7695*, 76950R.
35. Feygels, V.I.; Park, J.Y.; Wozencraft, J.; Aitken, J.; Macon, C.; Mathur, A.; Payment, A.; Ramnath, V. Czmil (coastal zone mapping and imaging lidar): From first flights to first mission through system validation. In Proceedings of the SPIE Defense, Security, and Sensing, Baltimore, MD, USA, 29 April–3 May 2013; pp. 1–15.
36. Kim, M.; Park, J.Y.; Tuell, G.H. A Constrained Optimization Technique for Estimating Environmental Parameters from CZMIL Hyperspectral and Lidar Data. In *Algorithms and Technologies for Multispectral, Hyperspectral, and Ultraspectral Imagery XVI*; SPIE: Bellingham, DC, USA, 2010; Volume 7695.
37. National Renewable Energy Laboratory; SMARTS: Simple Model of the Atmospheric Radiative Transfer of Sunshine. Available online: https://www.nrel.gov/grid/solar-resource/smarts.html (accessed on 1 October 2019).
38. Jensen, J.R. *Introductory Digital Image Processing: A Remote Sensing Perspective*; Prentice-Hall Inc.: Saddle River, NJ, USA, 1996.
39. Tuell, G.H.; Park, J.Y.; Aitken, J.; Ramnath, V.; Feygels, V.; Guenther, G.; Kopilevich, Y. SHOALS-enabled 3D benthic mapping. *Proc. SPIE* **2005**, *5806*, 816–826.
40. Copernicus Open Access Hub. Sentinel 2 Level 1C Imagery Processed by ESA. Available online: https://scihub.copernicus.eu/dhus/#/home (accessed on 28 January 2020).
41. Sentinel Application Platform (SNAP) [Computer Software]. Available online: https://step.esa.int/main/download/snap-download/ (accessed on 18 June 2020).
42. Song, C.; Woodcock, C.E.; Seto, K.C.; Lenney, M.P.; Macomber, S.A. Classification and change detection using Landsat TM data: When and how to correct atmospheric effects? *Remote Sens. Environ.* **2001**, *75*, 230–244. [CrossRef]
43. Serco Italia SPA. Sen2Coral Toolbox for Coral Reef Monitoring, Great Barrier Reef (Version 1.1). Available online: https://rus-copernicus.eu/portal/the-rus-library/learn-by-yourself/ (accessed on 18 June 2020).
44. Lyzenga, D.R. Passive remote sensing techniques for mapping water depth and bottom features. *Appl. Opt.* **1978**, *17*, 379–383. [CrossRef] [PubMed]
45. Green, P.E.; Mumby, P.J.; Edwards, A.J.; Clark, C.D. *Remote Sensing Handbook for Tropical Coastal Management*; UNESCO: Paris, France, 2000; p. 316.
46. Coastal and Marine Ecological Classification Standard. FGDC-STD-018-2012. Federal Geographic Data Committee. Reston, VA. Available online: https://www.fgdc.gov/standards/projects/cmecs-folder/CMECS_Version_06-2012_FINAL.pdf (accessed on 15 October 2019).
47. Strong, J.A.; Clements, A.; Lillis, H.; Galparsoro, I.; Bildstein, T.; Pesch, R.; Birchenough, S. A review of the influence of marine habitat classification schemes on mapping studies: Inherent assumptions, influence on end products, and suggestions for future developments. *ICES J. Mar. Sci.* **2019**, *76*, 10–22. [CrossRef]
48. Marine and Coastal Spatial Data Subcommittee. Coding System Approach for Coastal and Marine Ecological Classification Standard (CMECS) Classification and Modifier Units. In *Technical Guidance Document 2014-1*; Federal Geographic Data Committee: Reston, VA, USA, 2014; p. 8.
49. Marcello, J.; Eugenio, F.; Martin, J.; Marques, F. Seabed mapping in coastal shallow waters using high resolution multispectral and hyperspectral imagery. *Remote Sens.* **2018**, *10*, 1208. [CrossRef]
50. Congalton, R.G. A review of assessing the accuracy of classifications of remotely sensed data. *Remote Sens. Environ.* **1991**, *37*, 35–46. [CrossRef]
51. Reif, M.; Piercy, C.; Jarvis, J.; Sabol, B.; Macon, C.; Loyd, R.; Colarusso, P.; Dierssen, H.; Aitken, J. *Ground Truth Sampling to Support Remote Sensing Research and Development: Submersed Aquatic Vegetation Species Discrimination Using an Airborne Hyperspectral/Lidar System*; U.S. Army Engineer Research and Development Center: Vicksburg, MS, USA, 2012.
52. McCarthy, M.J.; Radabaugh, K.R.; Moyer, R.P.; Muller-Karger, F.E. Enabling efficient, large-scale high-spatial resolution wetland mapping using satellites. *Remote Sens. Environ.* **2018**, *208*, 189–201. [CrossRef]
53. Reif, M.K.; Theel, H.J. Remote sensing for restoration ecology: Application for restoring degraded, damaged, transformed, or destroyed ecosystems. *Int. Environ. Assess.* **2017**, *13*, 614–630. [CrossRef] [PubMed]
54. Poursanidis, D.; Traganos, D.; Reinartz, P.; Chrysoulakis, N. On the use of Sentinel-2 for coastal habitat mapping and satellite-derived bathymetry estimation using downscaled coastal aerosol band. *Int. J. Appl. Earth Obs. Geoinf.* **2019**, *80*, 58–70. [CrossRef]
55. Traganos, D.; Poursanidis, D.; Aggarwal, B.; Chrysoulakis, N.; Reinartz, P. Estimating satellite-derived bathymetry (SDB) with the google earth engine and sentinel-2. *Remote Sens.* **2018**, *10*, 859. [CrossRef]
56. Lu, D.; Weng, Q.A. Survey of image classification methods and techniques for improving classification performance. *Int. J. Remote Sens.* **2007**, *28*, 823–870. [CrossRef]

57. U.S. Geological Survey's TopoView. Available online: https://ngmdb.usgs.gov/topoview/viewer/ (accessed on 20 May 2021).
58. Abrams Aerial Survey Corporation. *Topographic Map of Illinois Beach Prepared for State of Illinois, Department of Conservation, Springfield Illinois. Scale 1:2.400*; Abrams Aerial Survey Corporation: Lansing, MI, USA, 1972.
59. Collinson, C. *House Falling in Water, Lake Michigan Shoreline, Zion, Illinois, April 1973: [35 mm Slide Scanned to JPG Format]*; Illinois State Geological Survey Photograph Collection, University of Illinois at Urbana-Champaign: Champaign, IL, USA, 1973.